

Copyright Warning & Restrictions

The copyright law of the United States (Title 17, United States Code) governs the making of photocopies or other reproductions of copyrighted material.

Under certain conditions specified in the law, libraries and archives are authorized to furnish a photocopy or other reproduction. One of these specified conditions is that the photocopy or reproduction is not to be “used for any purpose other than private study, scholarship, or research.” If a user makes a request for, or later uses, a photocopy or reproduction for purposes in excess of “fair use” that user may be liable for copyright infringement,

This institution reserves the right to refuse to accept a copying order if, in its judgment, fulfillment of the order would involve violation of copyright law.

Please Note: The author retains the copyright while the New Jersey Institute of Technology reserves the right to distribute this thesis or dissertation

Printing note: If you do not wish to print this page, then select “Pages from: first page # to: last page #” on the print dialog screen

The Van Houten library has removed some of the personal information and all signatures from the approval page and biographical sketches of theses and dissertations in order to protect the identity of NJIT graduates and faculty.

ABSTRACT

A MODEL FOR THERMAL DIFFUSION AND LOCAL TISSUE DAMAGE FROM THE MEASUREMENT OF TEMPERATURE IN ELECTROSURGICAL INCISION

**by
Marek Vira**

The extremely high temperatures applied over extremely short time intervals that are characteristic of electro-surgery result in a unique tissue damage pattern. Cesarean delivery and hysterectomy, the two most frequently performed procedures in obstetrics and gynecology (OB/GYN), commonly employ electro-surgical incision. While it is controversial, it has been suggested that tissue damage produced by electro-surgery could increase surgical site infection rates. While recommendations for the settings in the use of the electro-surgical unit do exist, there is no current technique for real time assessment of the viability of tissue around the site of the electro-surgical incision. Current methods for analyzing thermal damage inflicted on tissue are unsuitable for the case of electro-surgery as they do not match the temperature or time scales. In addition, minimal research has been performed on quantifying the temperature and resulting tissue damage in the vicinity of the electro-surgical incision.

Here, a noninvasive methodology that (1) accurately measures the heat generated by modern electro-surgical devices at the incision surface, (2) calculates the heat propagation into surrounding tissue, and (3) proposes a simple model for the estimation of the amount of tissue damage that occurs as a result of these thermal processes is proposed.

**A MODEL FOR THERMAL DIFFUSION AND LOCAL TISSUE
DAMAGE FROM THE MEASUREMENT OF TEMPERATURE IN
ELECTROSURGICAL INCISION**

**by
Marek Vira**

**A Thesis
Submitted to the Faculty of
New Jersey Institute of Technology
in Partial Fulfillment of the Requirements for the Degree of
Master of Science in Biomedical Engineering**

Department of Biomedical Engineering

August 2020

APPROVAL PAGE

**A MODEL FOR THERMAL DIFFUSION AND LOCAL TISSUE
DAMAGE FROM THE MEASUREMENT OF TEMPERATURE IN
ELECTROSURGICAL INCISION**

Marek Vira

Dr. George Collins, Thesis Advisor Date
Adjunct Professor of Biomedical Engineering, NJIT

Dr. Bruno Mantilla, Thesis Advisor Date
University Lecturer of Biomedical Engineering, NJIT

Dr. Bryan Pfister, Committee Member Date
Professor of Biomedical Engineering, NJIT

Dr. Max Roman, Committee Member Date
Research Professor of Biomedical Engineering, NJIT

BIOGRAPHICAL SKETCH

Author: Marek Vira

Degree: Master of Science

Date: August 2020

Undergraduate and Graduate Education:

- Master of Science in Biomedical Engineering,
New Jersey Institute of Technology, Newark, NJ, 2020
- Bachelor of Science in Biomedical Engineering,
New Jersey Institute of Technology, Newark, NJ, 2019

Major: Biomedical Engineering

Dedicated to all my failures.

ACKNOWLEDGMENT

Foremost, I would like to most graciously thank my advisors, Dr. George Collins and Dr. Bruno Mantilla for their unfailing support, invaluable guidance, and unending patience. I will miss their quirky banter and treasure their words of wisdom; I value their recommended reading and appreciate their powerful mentorship. I could not have asked for better advisors.

In addition, I would also like to express my sincere gratitude to my committee members Dr. Max Roman, for his continued interest in this thesis and his review of the computation portions, and Dr. Bryan Pfister, for his excitement and thorough questioning.

Special recognition goes to Dr. Kayaalp, who sparked this project, who inspired me every meeting, and who vouched so greatly for me at Hackensack Meridian Health Center -- allowing for the necessary tests to be completed.

Finally, without my beloved friends and family, I would not have been able to retain my nerve through the thesis process. I would like to specially thank my friends, Vivek Sreenivasan and Zackary Kellet, for their companionship on many long nights and during many long walks. I extend my heartfelt thanks to my family: my father, Jan, my mother, Alena, and my sister, Andrea. Their ceaseless love and compassion ensured I had all I needed, and more.

Without these individuals, this work would not have been possible. I am indebted to each one of them.

TABLE OF CONTENTS

Chapter	Page
1 INTRODUCTION.....	1
1.1 Objective	1
1.2 Background Information	1
2 EXPERIMENTAL METHODOLOGY.....	7
2.1 Physical Camera Setup.....	7
2.2 Processing Raw Camera Data.....	8
2.3 Use of Gelatin to Validate Computation Algorithm.....	9
2.4 Use of Porcine Pork Belly as Tissue Model.....	10
3 TEMPERATURE GRADIENT CALCULATION AND DAMAGE COMPUTATION AND RELATION.....	12
3.1 Temperature Gradient Calculation.....	12
3.2 Damage Computation and Relation.....	15
4 RESULTS.....	16
4.1 Gelatin Model Validation Results.....	16
4.2 Porcine Model Temperature Results.....	17
4.3 Tissue Damage Algorithm Results.....	33
5 DISCUSSION.....	38
6 CONCLUSION.....	40
7 FUTURE CONSIDERATION.....	41
APPENDIX A MATERIALS OUTLINE.....	42
APPENDIX B MATLAB CODES.....	43

TABLE OF CONTENTS
(Continued)

Chapter	Page
REFERENCES	48

LIST OF TABLES

Table	Page
2.3.1 First Trial Physical Thermocouple Locations and Their Corresponding Computed Cells.....	10
4.1.1 Positions of Physical Thermocouples and Their Corresponding Computed Elements.....	16
A.1 Properties of the Thermograph Camera	37
A.2 Properties of the Thermocouple Datalogger Thermometer.....	37
A.3 Properties of the Electrosurgery Equipment.....	37

LIST OF FIGURES

Figure	Page
1.2.1 General sinusoidal shape of the electrosurgical cutting waveform.....	5
1.2.2 Wattage vs peak voltage for electrosurgical waveforms.....	5
2.1.1 Physical camera setup with labeled components.....	7
2.2.2 Electroincision modeling user interface window.....	8
2.3.1 Thermocouple positions within the gelatin model.....	10
2.4.1 Thermocouple Positions within Gelatin Sample.....	11
3.1.1 Location of the elements and thermal conductances surrounding element $T_{i,j,k}$	13
4.1.1 Average of the validation results using a gelatin model and electrocautery pen...	17
4.2.1 Surface temperature data frames for an electroincision performed using the fulgurate function at 50W.....	18
4.2.2 Temperature data recorded from the first trial using the fulgurate function at 50W.....	19
4.2.3 Temperature data recorded from the second trial using the fulgurate function at 50W.....	20
4.2.4 Temperature data recorded from the third trial using the fulgurate function at 50W.....	21
4.2.5 Temperature data recorded from the fourth trial using the fulgurate function at 50W.....	22
4.2.6 Temperature data recorded from the fifth trial using the fulgurate function at 50W.....	23
4.2.7 Temperature data recorded from the first trial using the pure cut function at 30W.....	24
4.2.8 Temperature data recorded from the second trial using the pure cut function at 30W.....	25

LIST OF FIGURES
(Continued)

Figure	Page
4.2.9 Temperature versus time graph of the hottest point for an electroincision made using the fulgurate function at 50W and the cut function at 30W.....	26
4.2.10 Temperature data calculated in the plane of the electroincision from the first trial using the fulgurate function at 50W.....	27
4.2.11 Temperature data calculated in the plane of the electroincision from the second trial using the fulgurate function at 50W.....	28
4.2.12 Temperature data calculated in the plane of the electroincision from the third trial using the fulgurate function at 50W.....	29
4.2.13 Temperature data calculated in the plane of the electroincision from the fourth trial using the fulgurate function at 50W.....	30
4.2.14 Temperature data calculated in the plane of the electroincision from the fifth trial using the fulgurate function at 50W.....	31
4.2.15 Temperature data calculated in the plane of the electroincision from the first trial using the pure cut function at 30W.....	32
4.2.16 Temperature data calculated in the plane of the electroincision from the second trial using the pure cut function at 30W.....	33
4.3.1 Tissue viability for the first trial using the fulgurate function at 50W.....	34
4.3.2 Tissue viability for the second trial using the fulgurate function at 50W.....	34
4.3.3 Tissue viability for the third trial using the fulgurate function at 50W.....	35
4.3.4 Tissue viability for the fourth trial using the fulgurate function at 50W.....	35
4.3.5 Tissue viability for the fifth trial using the fulgurate function at 50W.....	36
4.3.6 Tissue viability for the first trial using the pure cut function at 30W.....	36
4.3.7 Tissue viability for the second trial using the pure cut function at 30W.....	37

LIST OF SYMBOLS

\approx	Approximately
∂	Partial Differential
$^\circ$	Degrees

LIST OF DEFINITIONS

Electroincision	Precise cut made using an electrosurgical device
Electrosurgery	Surgery using a high-frequency electric current to heat and so cut tissue
Thermograph	An instrument that produces a trace or image representing a record of the varying temperature or infrared radiation over an area or during a period of time

CHAPTER 1

INTRODUCTION

1.1 Objective

The goal of this thesis was to measure the surface temperature of a tissue model during electroincision and calculate, to a first approximation, the resultant temperature gradients throughout the tissue model. After validation of this computational methodology, an attempt was made to assess the viability of the tissue in the region of the electroincision.

1.2 Background Information

Cesarean delivery (CD) is the most common major surgical procedure performed in the United States. 1.2 million CDs are performed annually and account for 32% of all deliveries [1]. While CDs have become safer for the fetus, there are still significant risks for the mother. Most of the increased maternal risk of CD is associated with bleeding and infection. In addition to infection, wound separation accounts for further increase in complications for CD patients. A significant contribution to the increase in these complications is a change in the demographics of CD patients. Women have children later in life and have more health complications such as obesity, hypertension, and diabetes. The reported rate of surgical site infections (SSIs) for surgical procedures in general is 1.9%, while the rate of SSIs for CDs is much higher at 6.6%-10% [2, 3]. Surgical site infections resulting from Cesarean deliveries are estimated to cost the healthcare system \$182 million per year [4]. The increased implementation of CD procedures will unavoidably lead to an

increase in the number of cases with complications, thus impacting overall healthcare system costs.

Hysterectomy is the most common major gynecological surgery performed in the United States [5]. They are reported to have a postoperative surgical site infection rate of 22.6% [6]. Since the development of the electrosurgery unit in 1927, the popularity of the electrosurgery tool has greatly increased, becoming a standard surgical instrument in the operating room [7, 8]. Over 80% of surgical procedures now involve depositing thermal energy into tissue, resulting in a temperature increase in the surrounding tissue [9]. Given the rise in the use of electrosurgery tools and the rise of SSI and readmission rates in CDs and hysterectomies, the incentive of this research was a hypothesis that the degree of thermal injury caused by electrosurgery, during Cesarean deliveries and hysterectomies, could be a significant contributor to the observed wound complications. The presence of devitalized tissue favors bacterial growth and, consequently, raises SSI rates. Furthermore, higher thermal energy could potentially devitalize the tissue surrounding the incision, dead tissue could be inadvertently present at the end of the surgery, and subsequently produce a favorable environment for bacterial growth.

Modern electrosurgery units consist primarily of an alternating current power supply (such as a wall socket), regulatory circuitry, an active electrode, and a dispersive electrode [7]. The regulatory circuitry converts the low frequency current from the power supply to high frequencies, matching that of radiofrequencies [10]. Typically, the range of frequencies used is in the range of 1-3MHz, because when the frequency goes beyond 300kHz the faradic and electrolytic effects are eliminated, which results in the utilization of the high frequency thermal effect for both cutting and cauterization [8]. The high

concentration of current at the tip of the electrode produces extreme heating of the cells, which are torn apart by the boiling of the cell fluid [8]. It is important to note that the resulting effects of electrosurgery, cutting and cauterization, are caused by heat generated by coupling with dipolar structure of molecules in the tissue, in particular water. This type of tissue separation forms the basis of electrosurgical cutting [8]. Two major groups of electrosurgery devices exist, monopolar and bipolar. Monopolar tools require a grounding pad to complete the circuit and function. One of the most common monopolar tools is the “Bovie” pencil [11]. These instruments are named after William T. Bovie who invented the modern electrosurgical unit [12]. Bipolar tools work on the same principles as monopolar tools but are not limited by their need for a grounding pad, and, as such, are not only produced in the pencil design, but also in forceps and scissors designs, commonly found in laparoscopic electrosurgery tools [10]. As a model of electrosurgery, this work examines the heat generated during a monopolar electrincision, the type used in Caesarean delivery, and attempts to compute the thermal propagation and the resulting tissue damage.

A peak voltage of at least 200V is required to produce the necessary electric arc between the cutting electrode and the tissue. The peak voltage needed for use for cutting biological tissue is between 200V and 500V. When the peak voltage is greater than 500V, the electric arcs are so intense that the tissue is increasingly carbonized and the electrode tip may be damaged [8]. The term “coagulation” refers to the thermal fusion of the end of the severed blood vessels, and does not refer to the coagulation cascade. Although the specific details of the waveform and the spectrum used varies among electrosurgical generator manufacturers, the major waveform patterns used in electrosurgery are named cut, “coagulation,” blended, and fulguration [8, 9, 10]. The cutting waveform is a

continuous high frequency sinusoid with a relative lower peak voltage when compared to the other waveforms. The high current density aids in the vaporization of cells which, in turn, produces the cutting effect, but the low peak voltage often results in bleeding at the incision sight [9, 10]. The “coagulation” waveform is delivered as high voltage bursts separated by periods of isoelectric inactive segments. The blended waveform is a combination of the cut and “coagulation” waveforms. The fulgurate waveform has the highest peak voltage delivered in the smallest active time [8]. Fulguration is intended to be used by hovering the tip of the electrosurgical device above the tissue to release arcs of electricity from the tip, charring the tissue by dielectric breakdown [13]. Figure 1.2.1 shows the generic sinusoidal shapes of each of the waveforms. Figure 1.2.2 relates the wattage set on the electrosurgical generator to the peak voltage present at each setting. Here, “Cut 1” refers to the pure cut function and “Spray” refers to the fulgurate function.

It has been observed that surgeons often set the electrosurgical generators beyond the recommended settings [Emre Kayaalp, personal communication, February 24, 2020]. The recommended electrosurgical generator settings for general gynecological operation are 30W on both the cut waveform and the fulgurate waveform. [Emre Kayaalp, personal communication, February 24, 2020]. The electrosurgical cut is made using the cut function, and any resulting bleeding is “coagulated” using the fulgurate function. Frequently, the electrosurgical cut is not made using the pure cut waveform at 30W, but rather using the fulgurate setting at 50W [Emre Kayaalp, personal communication, February 24, 2020]. The use of the fulgurate waveform at higher wattages for the purpose of cutting may sever the tissue and prevent bleeding, but it also elicits an increased amount of thermal energy into the tissue when compared to using the cut function at lower wattages. In an anecdotal

observation charred tissue build up on the tool increases resistance, limiting effective cutting of the tool, requiring more power to obtain the same result and increasing the temperature in surrounding tissue

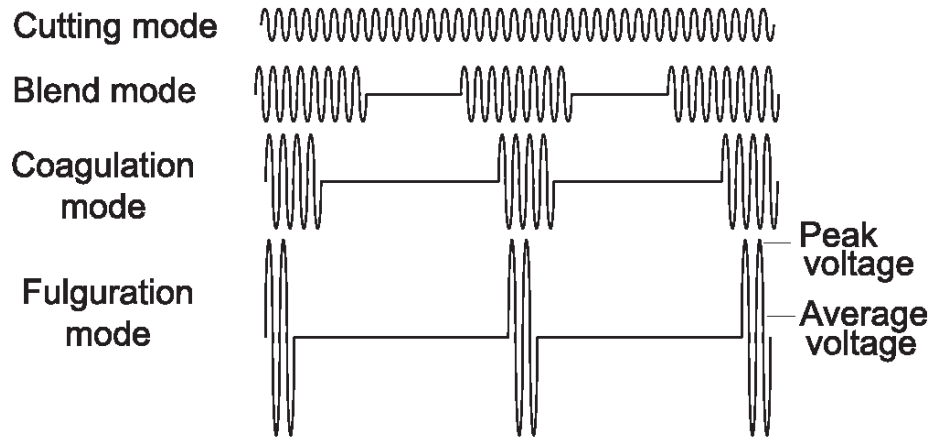


Figure 1.2.1 General sinusoidal shape of the electro-surgical cutting waveform [14].

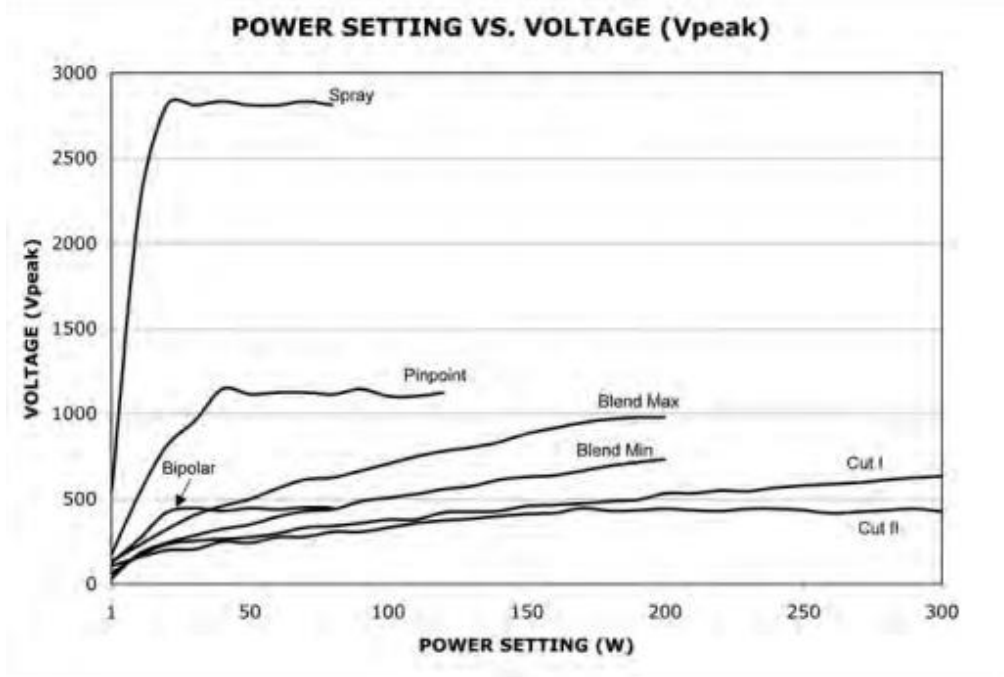


Figure 1.2.2 Wattage vs peak voltage for electro-surgical waveforms [15].

This combination of both extreme and rapid temperature increase produces an injury pattern that is characteristic of electro-surgery. Though it is a topic of growing

interest, minimal research has been performed to explore injury caused by electrosurgery and its consequences. No previous analysis could be identified that attempted to describe the heat generation and tissue damage in real time during an electroincision. This work attempts to produce a model that can compute the temperature and relate that temperature to tissue damage. Further, this work attempts to combine the medical-biological assessment with quantitative engineering approach by computing temperature and damage during an electroincision. While the long-term effects of temperature increase on tissue have been well researched and observed, there is minimal understanding about the effects of short bursts of high temperature increase in tissue. Some studies have found that the use of electrosurgical equipment during an operation can double the rate of post-operative infection, while others claim no difference between surgeries that employed electrosurgery and surgeries that did not [16, 17, 18]. In addition, it been speculated that the complications that arise from electrosurgery are underreported [19].

CHAPTER 2

EXPERIMENTAL METHODOLOGY

2.1 Physical Camera Setup

A FLIR C2 thermograph camera with a resolution of 60x80 pixels and a capture rate of 15 frames per second was used to collect the surface temperature data near the electroincision. A camera stand was used to affix the thermograph camera in the proper placement during testing. The camera was held directly above the tissue model at a height of approximately fifty-three centimeters from the base of the model to minimize the impact of the camera's presence on the operator's ability to use the electrosurgery device. A level was used to ensure the plane of the thermograph camera was nominally placed parallel to the plane of the tissue models to achieve the most accurate calculation. Data from the camera was transferred to, and stored on, the computer via a micro-USB wire connecting the camera and computer. Figure 2.1.1 shows an image of the physical camera setup. The individual components are labeled in red.

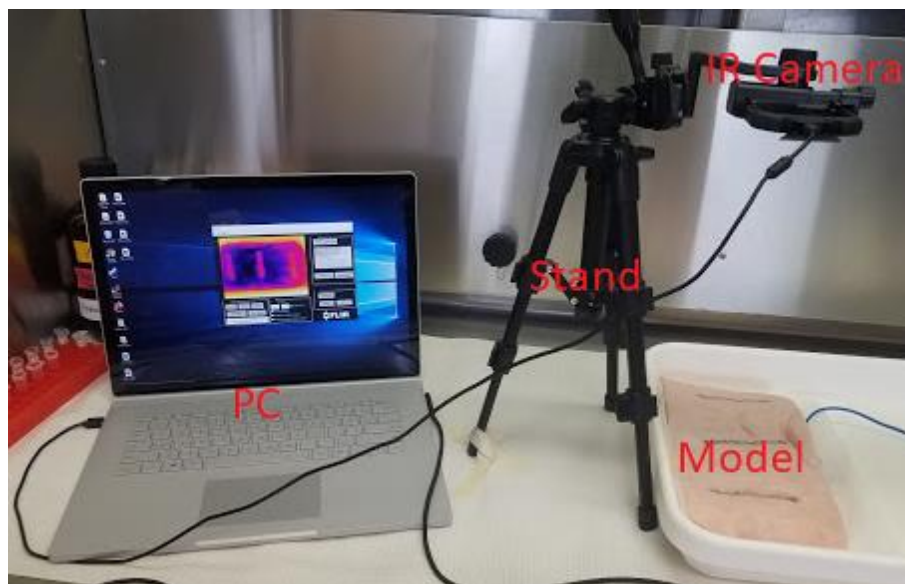


Figure 2.1.1 Physical camera setup with labeled components.

2.2 Processing Raw Camera Data

Data collection was initiated using a proprietary software, named “GUITest.m” provided by the camera manufacturer. During this process, pixel-by-pixel temperature data from the camera was transferred to, and stored on, the computer in a proprietary “.seq” file format. A MATLAB algorithm was created to translate the data from this proprietary file format to a “.mat” file containing the pixel-by-pixel temperature data in degrees Celsius. MATLAB was used for this data collection and processing because the manufacturer’s support for the thermograph camera in this coding language created a streamlined data collection process. A user interface was developed in MATLAB to collect all of the processing, calculation, data management, and data viewing functions into a single, intuitive program. Animations of the electroincision at any plane can be played, or the planes can be studied more closely by viewing each time step individually. Figure 2.1.2 illustrates the user interface window.

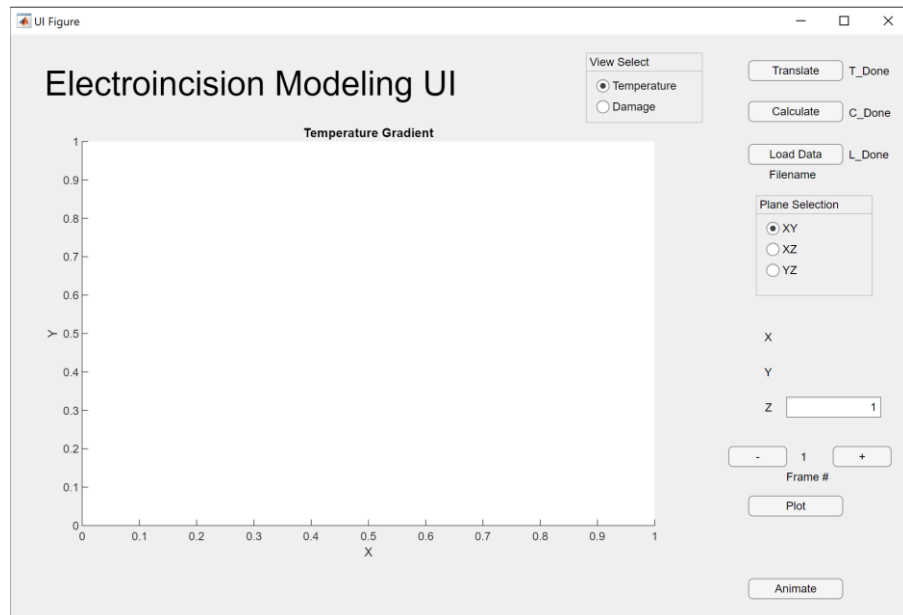


Figure 2.2.2 Electroincision modeling user interface window.

2.3 Use of Gelatin to Validate Computation Algorithm

Because the current from an electrosurgical device would damage a thermocouple data logger, an electrocautery device that generates heat but no current was used for computational validation. Because gelatin offers facile placement of thermocouples, a gelatin model was used for computational validation. The dimensions of the gelatin model were 16cm by 24cm by 1cm. Figure 2.3.1 depicts the placements of the thermocouples and Table 2.3.1 relates the physical locations of the thermocouples to their corresponding volumetric elements. The electrocautery incisions were made along the route of the thermocouples. Meaning that, for the first trial, the incision begins at approximately 5cm in the x axis and 3cm in the y axis, and ends at approximately 9cm in the x axis and 3cm in the y axis. The x axis positions of the thermocouples were kept at a constant distance 1.25cm between them throughout all the trials. The z axis positions were placed 0.2cm, 0.3cm, 0.4cm and 0.5cm from the surface. The thermocouples were translated three centimeters along the y axis of the gelatin model after each incision was performed, resulting in six trials being performed.

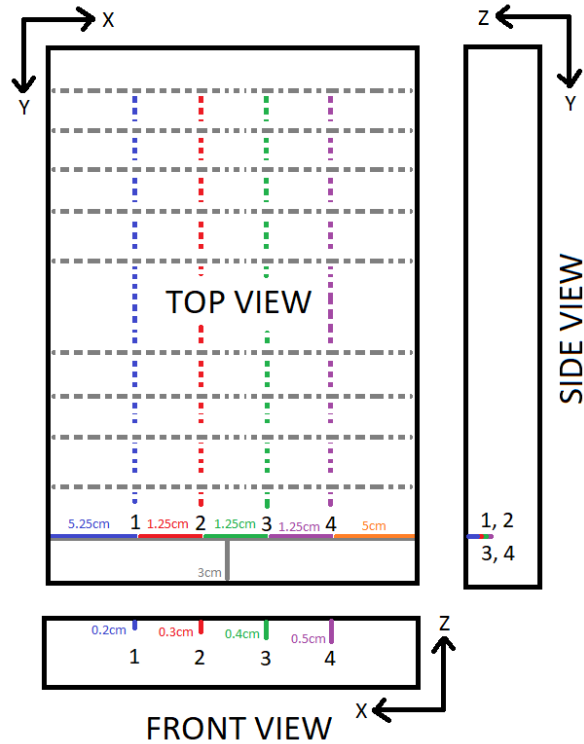


Figure 2.3.1 Thermocouple positions within the gelatin model.

Table 2.3.1 First Trial Physical Thermocouple Locations and Their Corresponding Computed Cells

Thermocouple Number	Thermocouple Position (x, y, z)cm	Corresponding Computed Elements (i, j, k)
1	5.3, 3, 0.2	20, 10, 2
2	6.5, 3, 0.3	24, 10, 3
3	7.8, 3, 0.4	29, 10, 4
4	9, 3, 0.5	34, 10, 5

2.4 Use of Porcine Pork Belly as Tissue Model

A porcine tissue was used as the tissue model in the testing, because it has been accepted and used as model for human tissue. Studies show that various parts of the porcine tissue mimic human tissue quite well, especially areas such as the skin [20, 21]. A ten-pound slab of pork belly was purchased and stored at a temperature of 15°C until it was cut into pieces

measuring 16x24cm prior to testing. The thickness of these pieces was 3cm. 6cm length electroincisions were made on the surface, with an estimated depth of 0.3cm. The incisions were separated 4.5cm from each other. As seen in Figure 2.4.1, the red lines indicate incisions performed using the fulgurate function and the blue lines indicate incisions performed with the pure cut function.

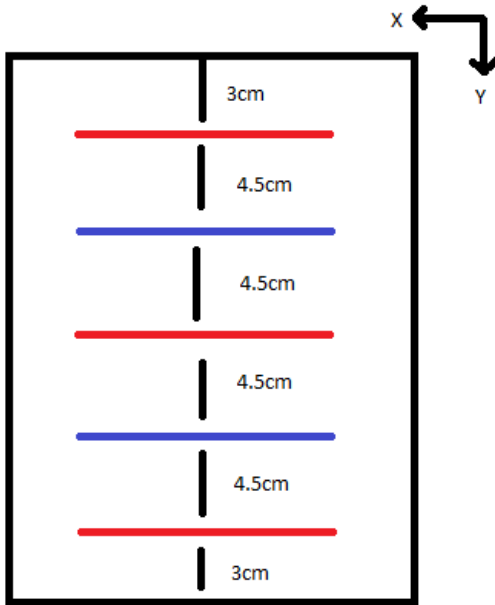


Figure 2.4.1 Locations of 6cm electroincisions in pork belly model.

CHAPTER 3

TEMPERATURE GRADIENT CALCULATION AND DAMAGE

COMPUTATION AND RELATION

3.1 Temperate Gradient Calculation

The equation used to compute the temperature gradients is derived from the heat conduction equation in three dimensions [22]. The heat conduction equation is shown in equation 1.1.

$$\frac{\partial}{\partial x} \left(\lambda_x \frac{\partial T}{\partial x} \right) + \frac{\partial}{\partial y} \left(\lambda_y \frac{\partial T}{\partial y} \right) + \frac{\partial}{\partial z} \left(\lambda_z \frac{\partial T}{\partial z} \right) + I(x, y, z, t) = C \frac{\partial T}{\partial t} \quad (1.1)$$

On the left side of the heat conduction equation are the second partial derivatives of temperature in relation each of the axes multiplied by their respective thermal conductance value, λ . Because the only source of temperature increase in the trials is the electrosurgery tool, the I term in equation 1.1, which represents internal heat generation, is considered 0, and thus not mentioned moving forward. On the right side of the equation is the partial derivative of temperature in relation to time multiplied by heat capacity, C . Equation 1.2 shows the discretized form of the heat conduction equation.

$$T_{i,j,k}^{t+1} = T_{i,j,k}^t + \frac{\Delta t}{C_{i,j,k} \Delta x_i \Delta y_j \Delta z_k} \cdot H_{i,j,k} \quad (1.2)$$

$T_{i,j,k}^{t+1}$, the temperature at the next time step, is equal to $T_{i,j,k}^t$, the temperature at the previous time step, plus the heat through all surrounding volumetric elements, defined as Δt , the time step, divided by $C_{i,j,k}$, the heat capacity, multiplied by $\Delta x_i \Delta y_j \Delta z_k$, the volume

of the element. The heat from all the surrounding elements, $H_{i,j,k}$, is determined by subtracting the temperature of the element, $T_{i,j,k}$, from the respective surrounding temperatures and multiplying by the respective K value. The equation is shown in equation 1.3 and the positions of the surrounding volume elements and K values of the central element, $T_{i,j,k}$, are shown in Figure 3.1.1.

$$\begin{aligned}
 H_{i,j,k} = & K_{i-\frac{1}{2},j,k} (T_{i-1,j,k} - T_{i,j,k}) + K_{i+\frac{1}{2},j,k} (T_{i+1,j,k} - T_{i,j,k}) \\
 & + K_{i,j-\frac{1}{2},k} (T_{i,j-1,k} - T_{i,j,k}) + K_{i,j+\frac{1}{2},k} (T_{i,j+1,k} - T_{i,j,k}) \\
 & + K_{i,j,k-\frac{1}{2}} (T_{i,j,k-1} - T_{i,j,k}) + K_{i,j,k+\frac{1}{2}} (T_{i,j,k+1} - T_{i,j,k})
 \end{aligned} \tag{1.3}$$

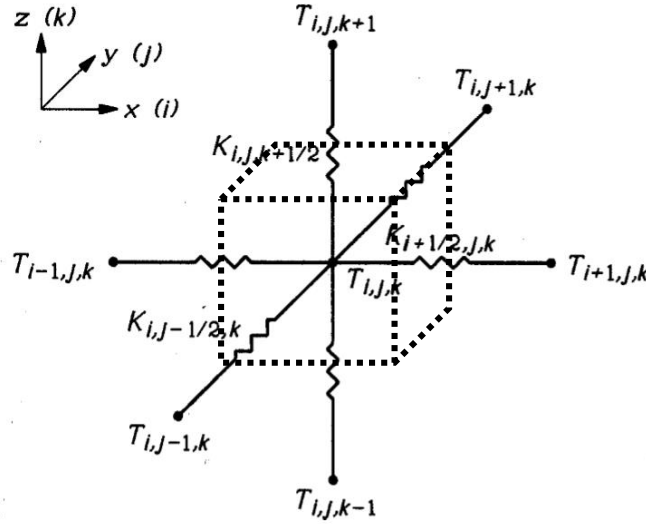


Figure 3.1.1 Location of the elements and thermal conductances surrounding element $T_{i,j,k}$ [22].

An example for the calculation of $K_{i,j,k+\frac{1}{2}}$ is shown in equation 1.4. It is equal to Δx_i , the element length in the x axis, multiplied by Δy_j , the element length in the y axis, divided by the ratio of Δz_k , the length of the element in the z axis, to two times the respective thermal conductance value, $\lambda_{i,j,k}$, plus the ratio of $_$ plus the resistance value,

$R_{i,j,k+\frac{1}{2}}$, between the element i,j,k and the element $i,j,k+1$.

$$K_{i,j,k+\frac{1}{2}} = \frac{\Delta x_i \Delta y_j}{\frac{\Delta z_k}{2\lambda_{i,j,k}} + \frac{\Delta z_{k+1}}{2\lambda_{i,j,k+1}} + R_{i,j,k+\frac{1}{2}}} \quad (1.4)$$

By adjusting the subscripts of K , the summation of the K values can be found, as shown in equation 1.5.

$$\sum K = K_{i-\frac{1}{2},j,k} + K_{i+\frac{1}{2},j,k} + K_{i,j-\frac{1}{2},k} + K_{i,j+\frac{1}{2},k} + K_{i,j,k-\frac{1}{2}} + K_{i,j,k+\frac{1}{2}} \quad (1.5)$$

$\sum K$ can then be used to calculate the heat capacity value, $C_{i,j,k}$, as show in equation 1.6.

$$C_{i,j,k} = \Delta t \cdot \frac{\sum K}{\Delta x_i \Delta y_j \Delta z_k} \quad (1.6)$$

The porcine tissue sample was considered to be homogenous, and so all values of the thermal conductivity constant, λ , were taken as equal. The thermal conductivity constant, λ , used for the tissue sample was 0.23 W/(m·K), a value obtained from previous research [23]. The data obtained from the thermograph camera was used as the boundary condition for the top surface of the calculation, a previously obtained value for the atmospheric temperature was used as the boundary condition for the side surfaces of the calculation, and the starting sample temperature was used as the bottom surface boundary condition. The starting temperature of the whole model, in both the gelatin and pork belly, besides the surface layer, was also set to the initial temperature of the surface without any perturbation. The equation was then applied iteratively for every point within the three-dimensional matrix for every frame of thermograph video collected. Keeping the plane of the thermograph camera parallel to the plane of the surface of the model was crucial

because any tilt would cause a misalignment in the axes of the calculation and the axes of the model. Minor deformities on the surface of the samples were considered negligible for the purposes of calculation. While the hand of the operator and basic shape of the monopolar pen can be seen in the thermograph recording, computationally, these temperature increases are disregarded, as they are far below the interest of this work.

3.2 Damage Computation and Relation

While the long-term effects of temperature increase on tissue have been well researched and observed, there is minimal understanding about the effects of short bursts of high temperature increase in tissue. One commonly found assessment, in literature, is the damage produced by prolonged exposure of 43°C and higher, and has originated the quantification scales of the changes within the tissue, usually referred to as cumulative equivalent minutes at 43°C [24]. This method is unsuitable for an injury pattern that can exceed temperatures over 80°C and occurs on second timescale. As a result, an alternative examination of the tissue viability is achieved through the application of temperature thresholds. At 60°C cells instantly die due to desiccation [11]. At 45°C the denaturation of the cellular proteins becomes important [25]. Using this information, volumetric elements were labeled according to their tissue viability. It is assumed that elements that do not exceed 45°C represent healthy tissue, elements that surpass 45°C but stay below 60°C sustain cumulative damage, and elements that pass 60°C represent dead tissue.

CHAPTER 4

RESULTS

4.1 Gelatin Model Validation Results

A thermal conductivity value of $.30 \text{ W}/(\text{m}\cdot\text{K})$ was obtained from the literature for the gelatin model [26]. That thermal conductivity value was empirically adjusted to a value of $0.29 \text{ W}/(\text{m}\cdot\text{K})$ so that the computed values better fit the experimental values. Figure 4.1 displays the average temperature of six trials versus time of both the recorded thermocouple temperature, in red, and the computed temperature, in blue. Temperature was determined at six positions along the y axis and averaged.

Table 4.1.1 Positions of Physical Thermocouples and Their Corresponding Computed Elements

Thermocouple Number	Thermocouple Position (x, y, z)cm	Corresponding Computed Elements (i, j, k)
1	5.3, y, 0.2	20, j, 2
2	6.5, y, 0.3	24, j, 3
3	7.8, y, 0.4	29, j, 4
4	9, y, 0.5	34, j, 5

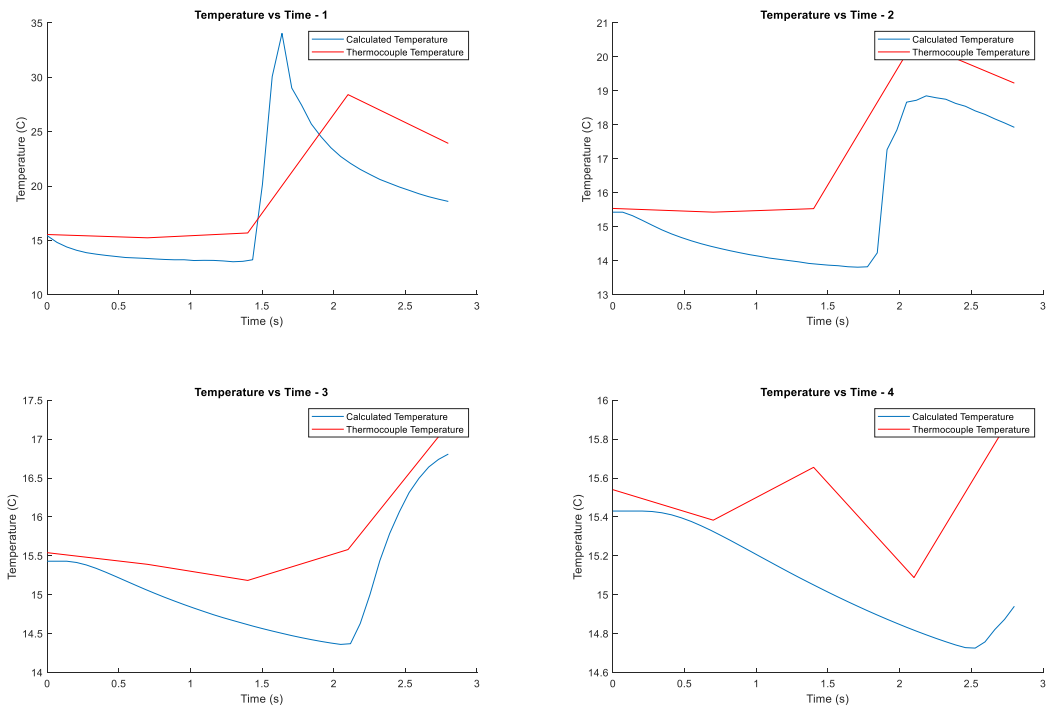


Figure 4.1.1 Average of the validation results using a gelatin model and electrocautery pen.

Although the computation does not fit the experimental results well, this might arise from the difference in sampling rate between the thermograph camera, 15 frames per second, and the thermocouple data logger, 2 values per second. This difference could not be resolved, and in as much as these curves are nominally the same shape, they were accepted as reasonable correspondence.

4.2 Porcine Model Temperature Results

Each volumetric element in the results represents an area 3mm by 2.7mm, or 8.1mm^2 and a volume of 3mm by 2.7mm by 3mm, or a volume of 24.3mm^3 . The site of the electroincision has been zoomed in to more clearly show the individual elements. Figure 4.2.1 shows all the frames of the electroincision performed using the fulgurate function at

50W.

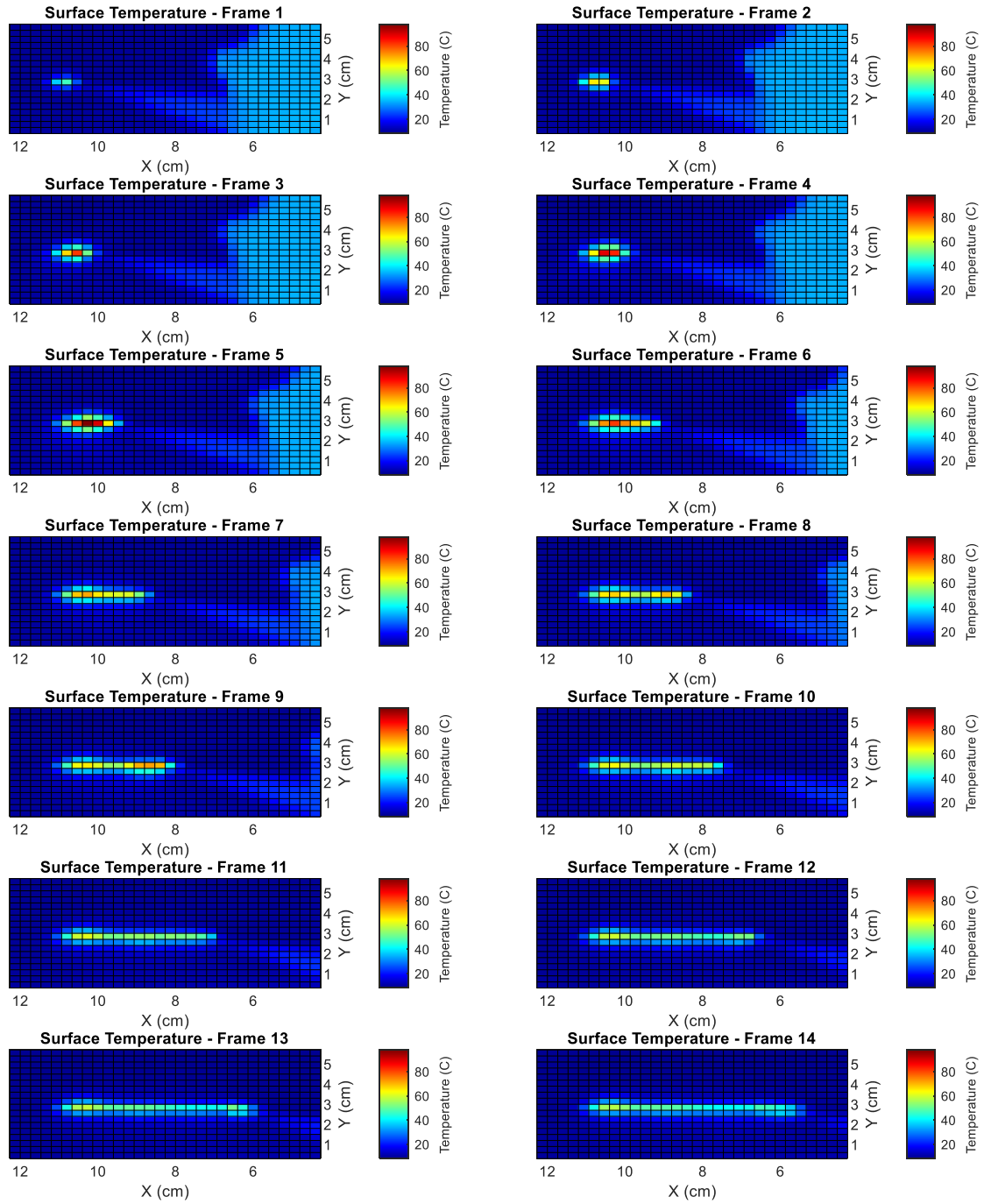


Figure 4.2.1 Surface temperature data frames for an electroincision performed using the fulgurate function at 50W.

Figure 4.2.2 through Figure 4.2.6 show the surface temperatures at the start point of the electroincision, during a midpoint of the electroincision, and at the end point of the electroincision for the trials made using the fulgurate function set to 50W. Here, red coloring indicates temperatures around 80°C and the blue coloring indicates temperatures around 15°C.

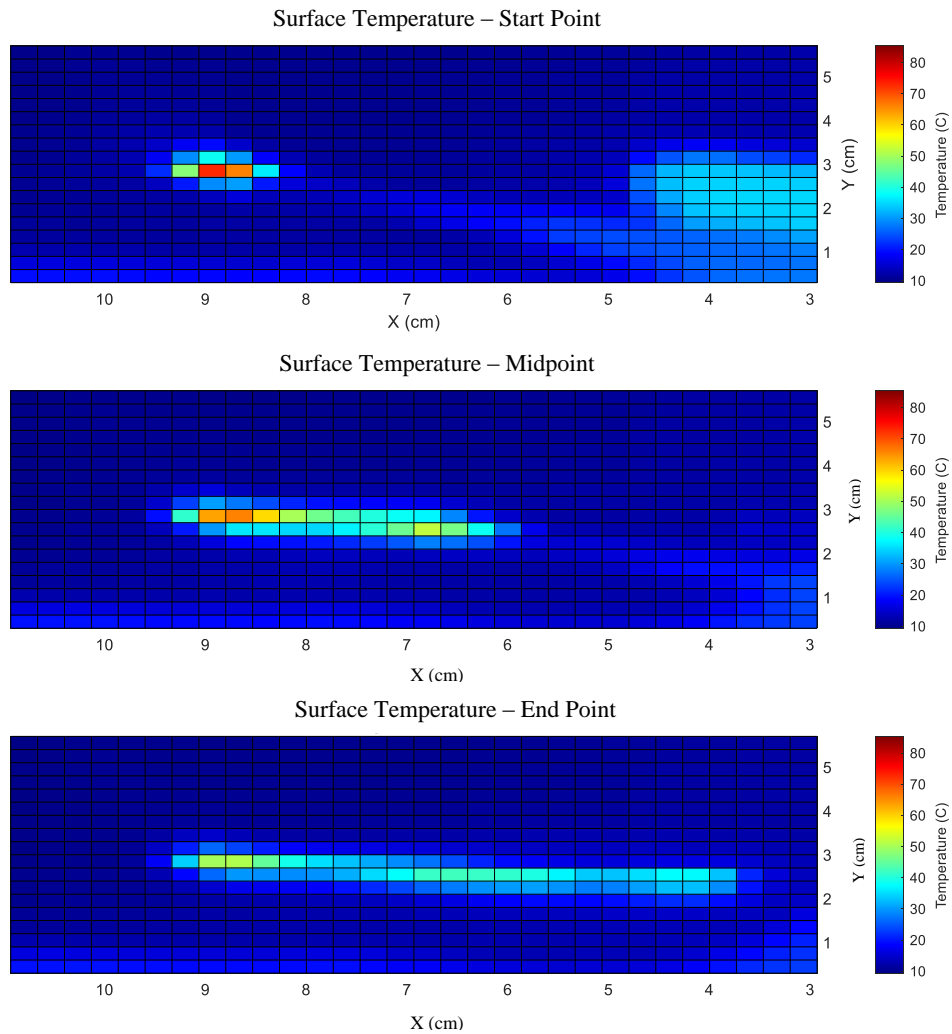


Figure 4.2.2 Temperature data recorded from the first trial using the fulgurate function at 50W.

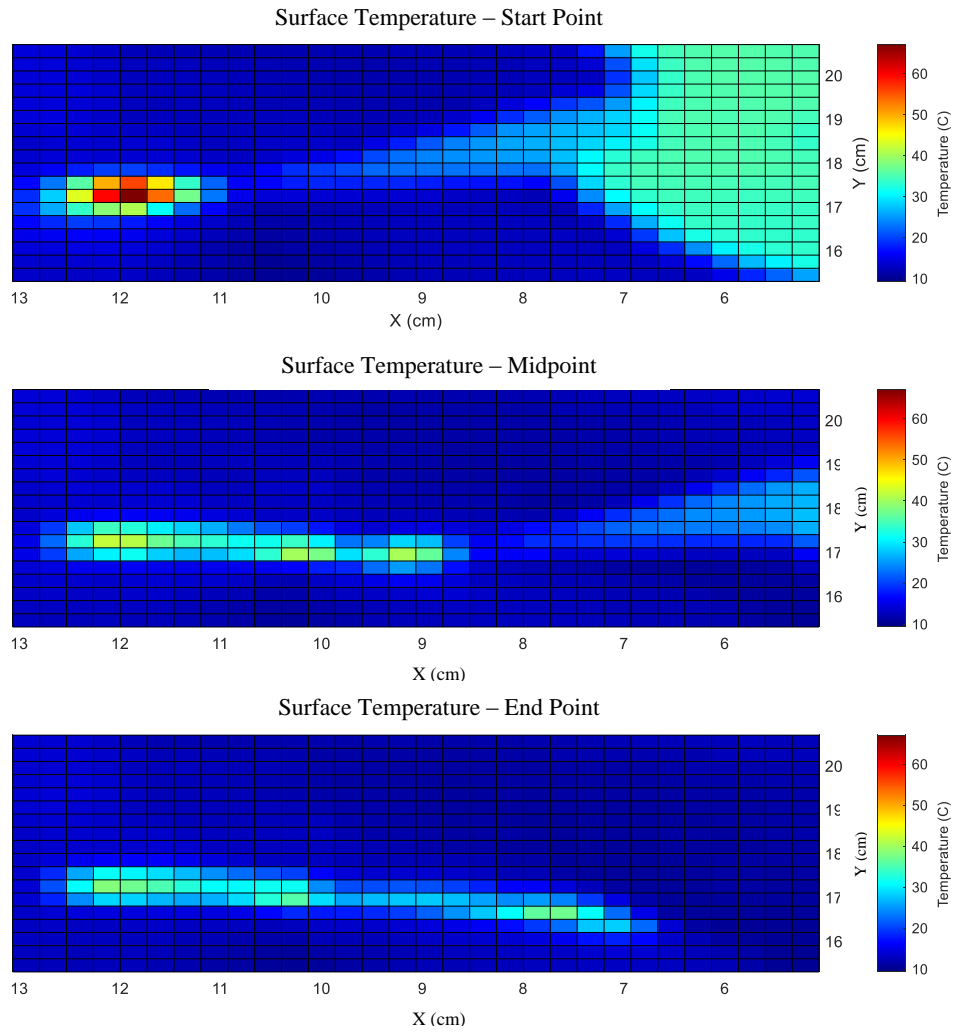


Figure 4.2.3 Temperature data recorded from the second trial using the fulgurate function at 50W.

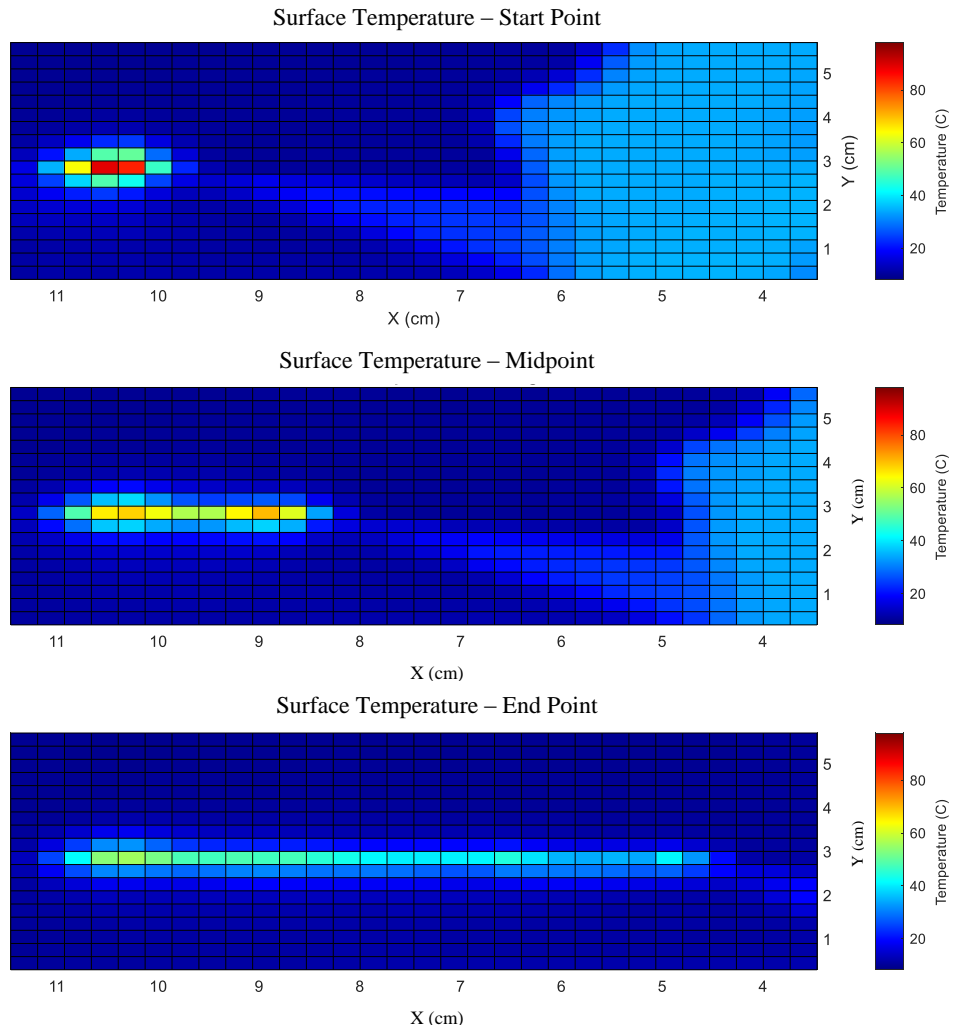


Figure 4.2.4 Temperature data recorded from the third trial using the fulgurate function at 50W.

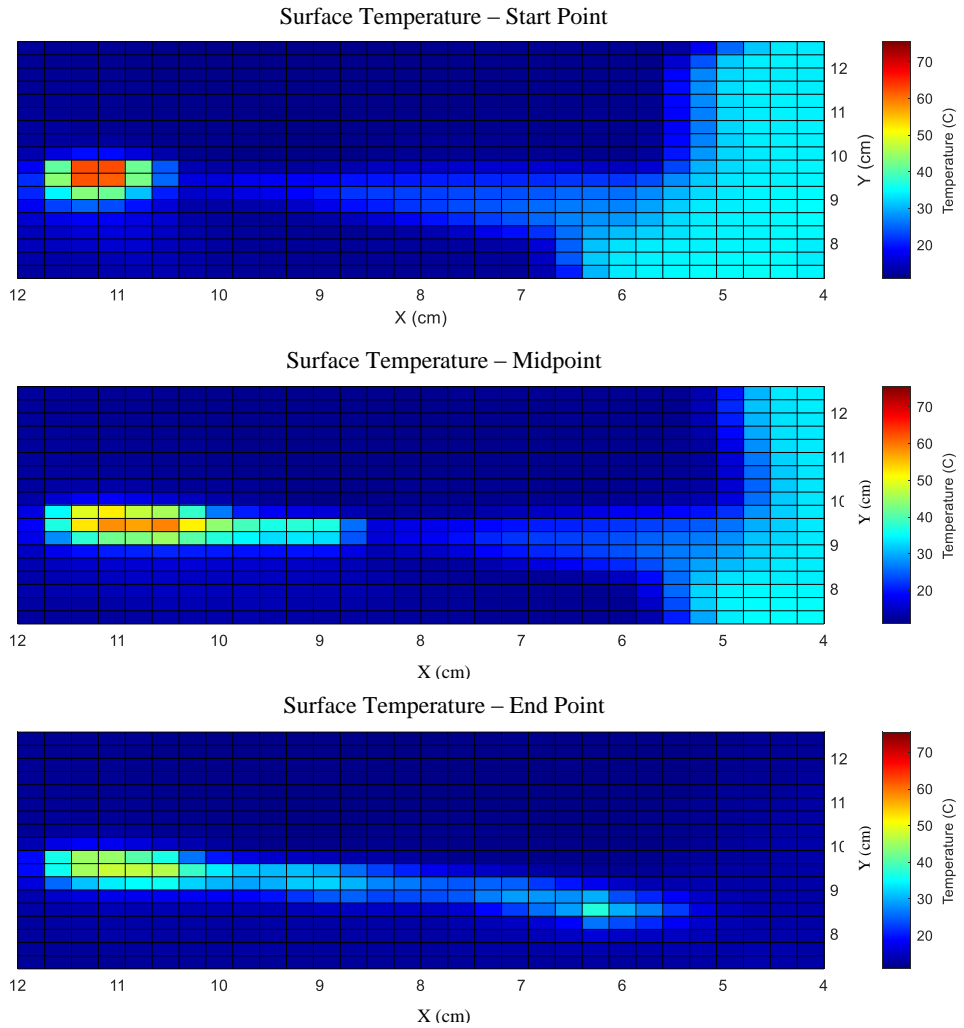


Figure 4.2.5 Temperature data recorded from the fourth trial using the fulgurate function at 50W.

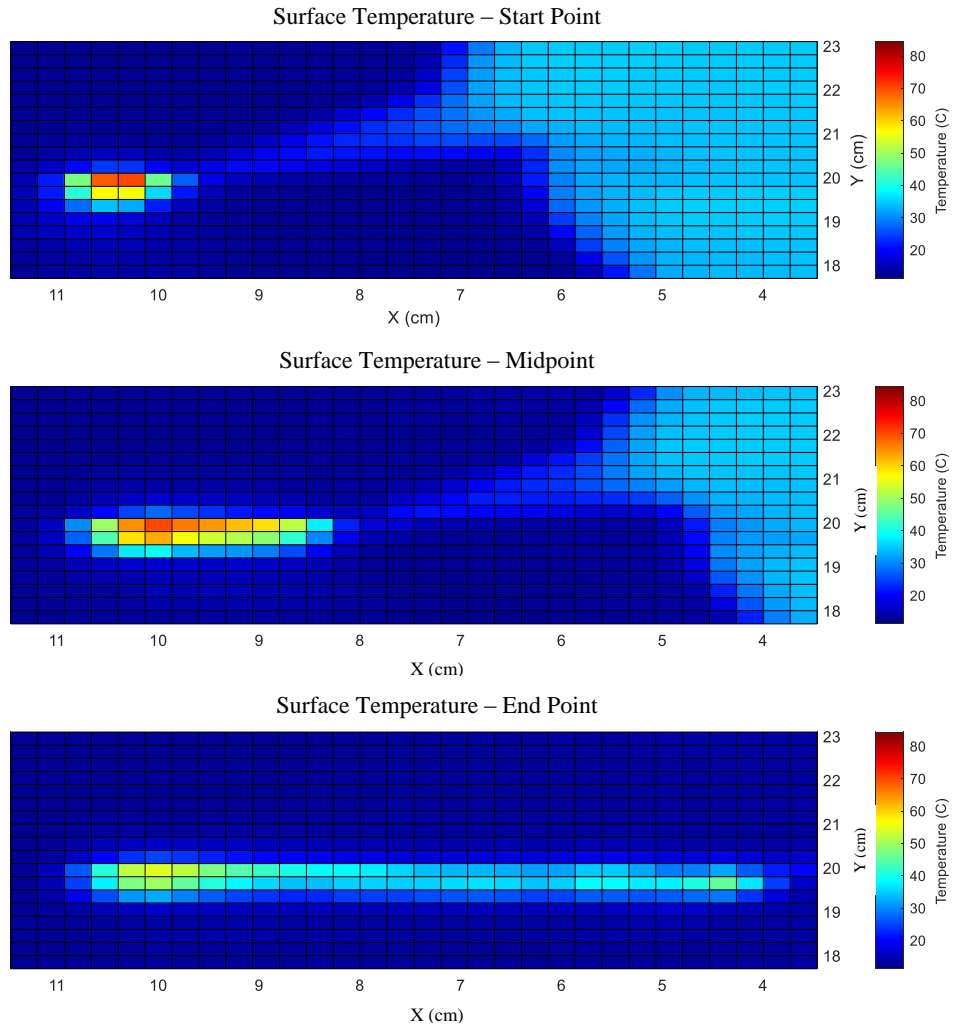


Figure 4.2.6 Temperature data recorded from the fifth trial using the fulgrate function at 50W.

Figure 4.2.7 and Figure 4.2.8 show the surface temperatures at the initiation of the electroincision, during a midpoint of the electroincision, and during the conclusion of the electroincision for the trials made using the pure cut function set to 30W. Red coloring indicates temperatures around 35°C and blue coloring indicates temperatures around 10°C.

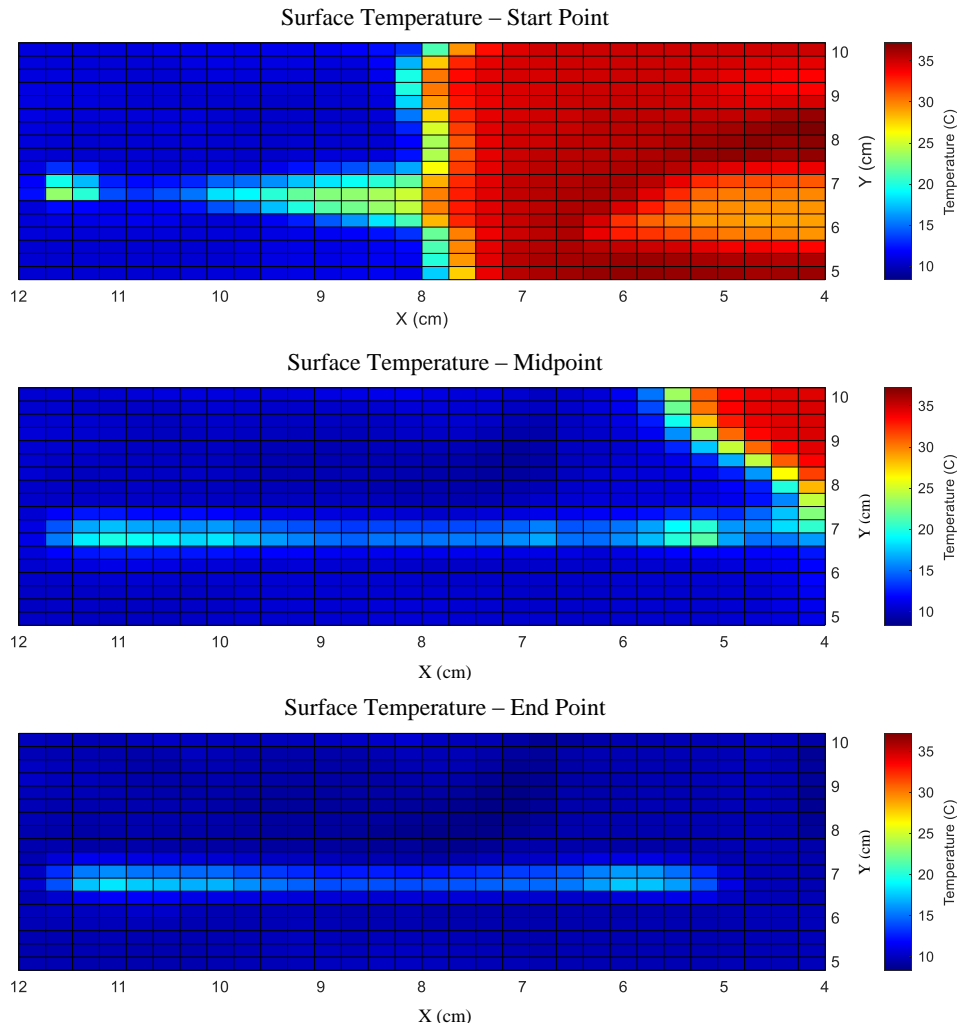


Figure 4.2.7 Temperature data recorded from the first trial using the pure cut function at 30W.

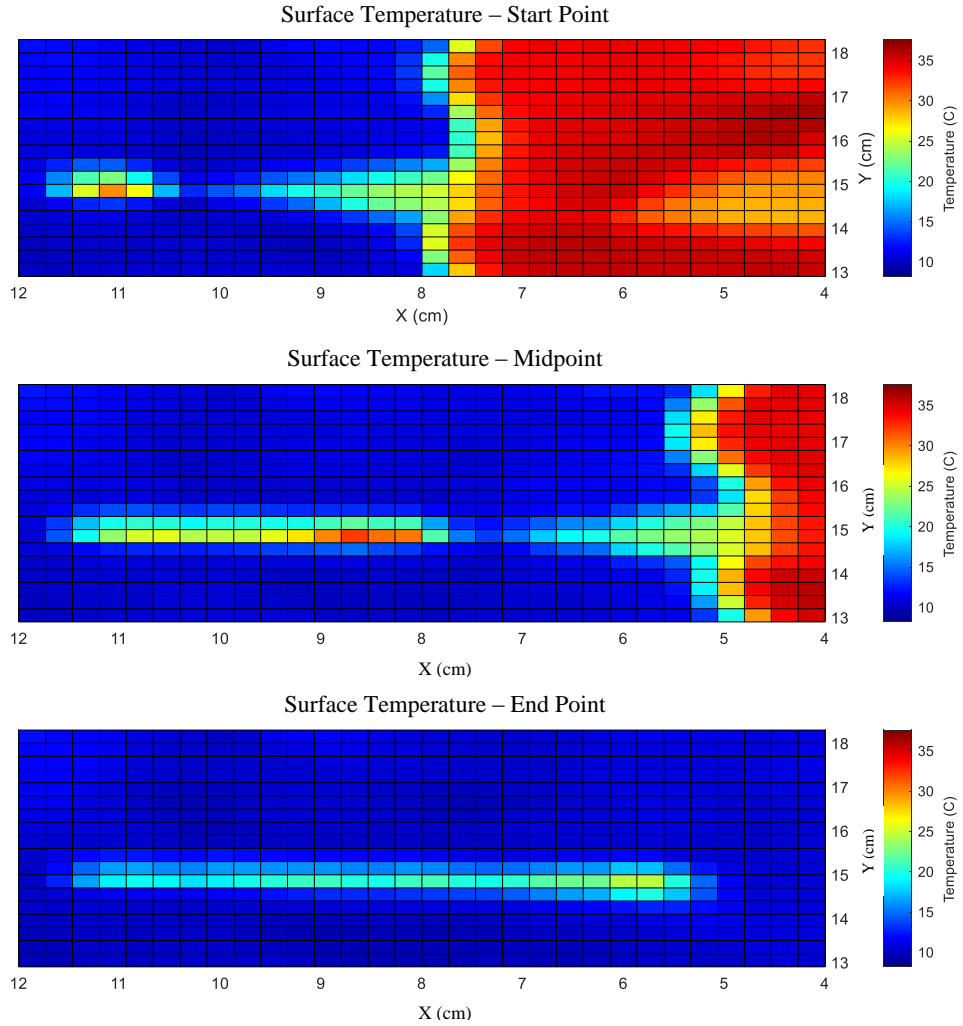


Figure 4.2.8 Temperature data recorded from the second trial using the pure cut function at 30W.

Figure 4.2.9 displays the temperature of the hottest computational volume elements in both a trial using increased settings, the fulgurate function at 50W, in blue, and a trial using the recommended settings, the cut function at 30W, in red.

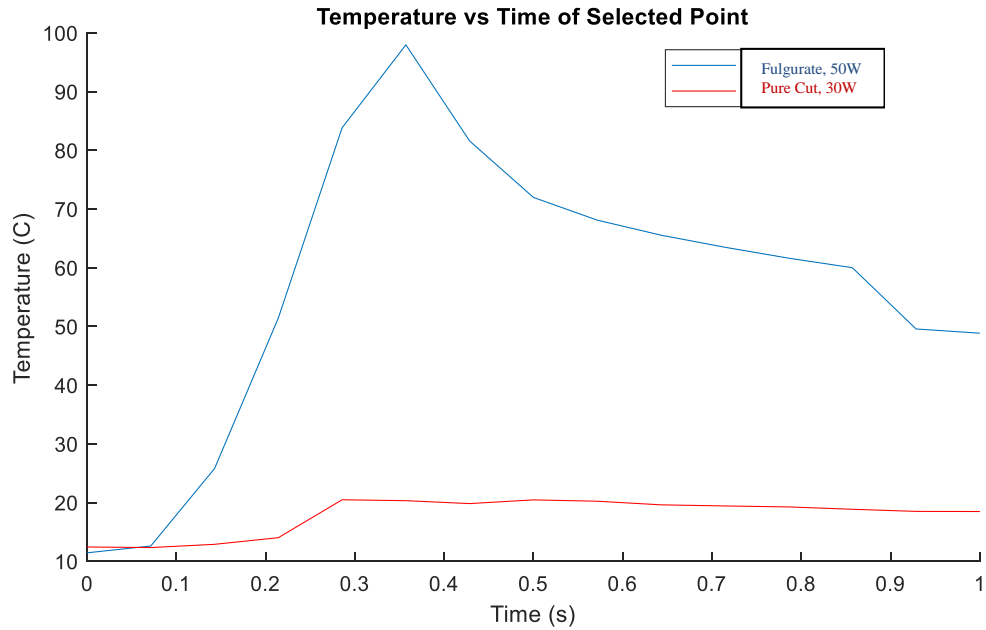


Figure 4.2.9 Temperature versus time graph of the hottest point for an electroincision made using the fulgurate function at 50W and the cut function at 30W.

Figure 4.2.10 through Figure 4.2.14 show the temperatures gradient in the x-z plane along the electroincision at the initiation of the electroincision, during a midpoint of the electroincision, and during the conclusion of the electroincision for the trials made using the fulgurate function set to 50W. Red coloring indicates temperatures around 80°C and blue coloring indicated temperatures around 15°C.

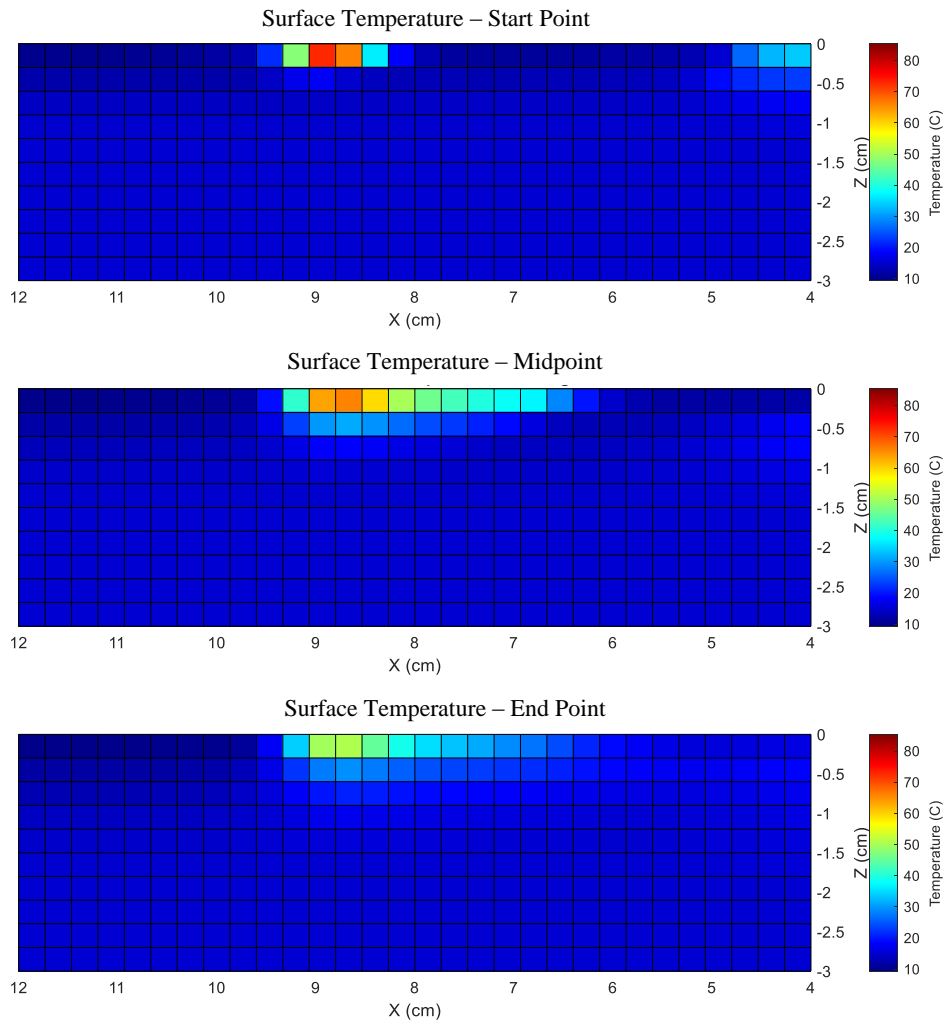


Figure 4.2.10 Temperature data calculated in the plane of the electroincision from the first trial using the fulgurate function at 50W.

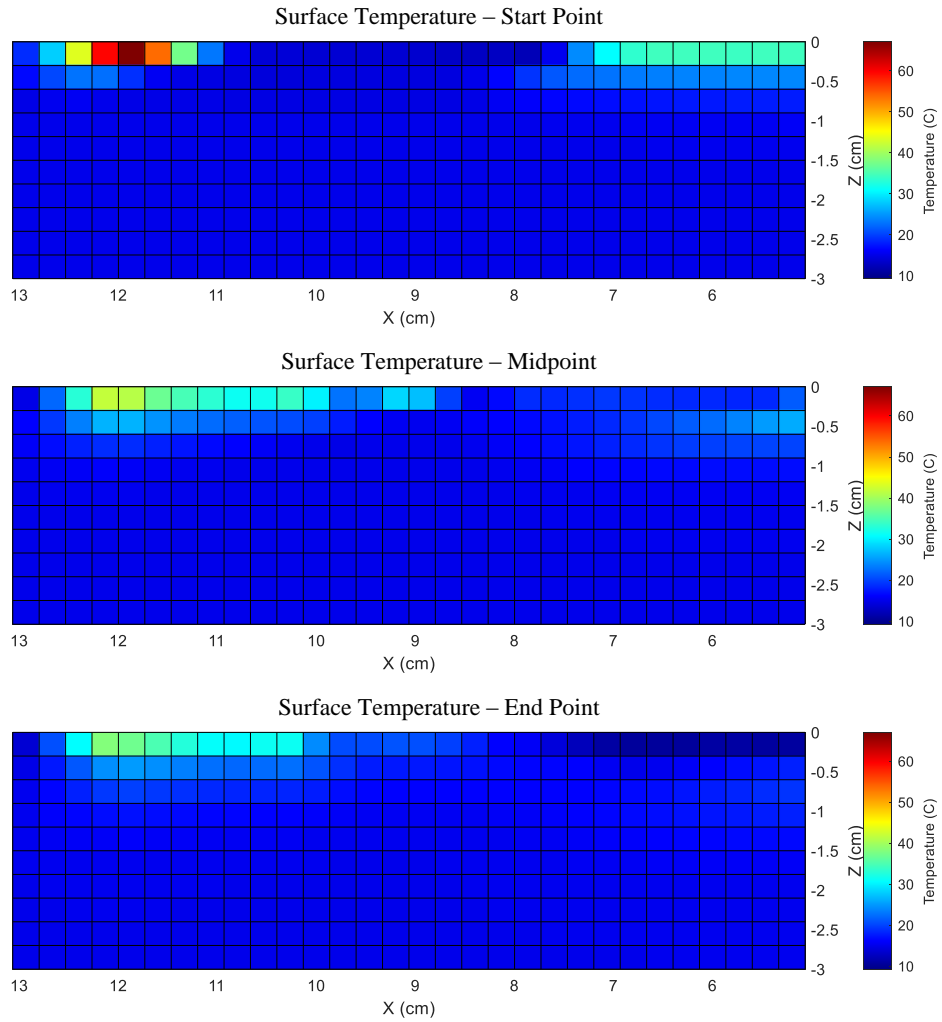


Figure 4.2.11 Temperature data calculated in the plane of the electroincision from the second trial using the fulgurate function at 50W.

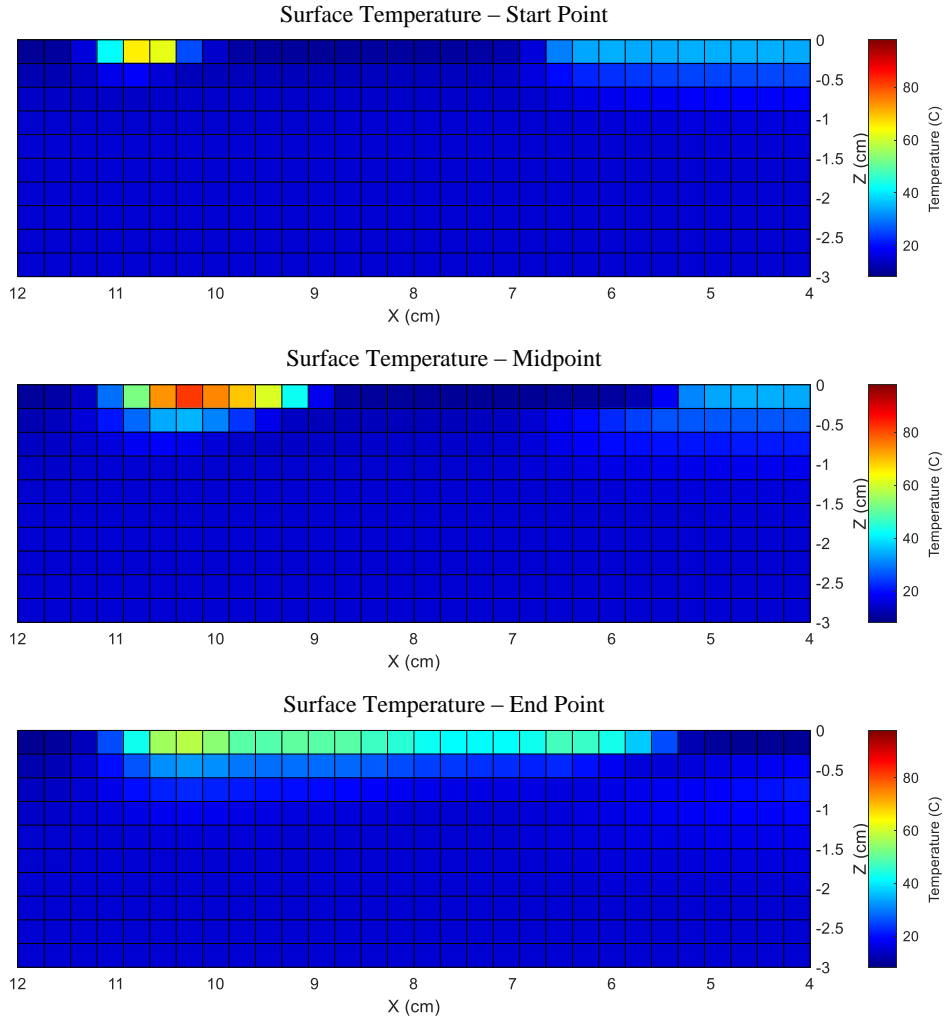


Figure 4.2.12 Temperature data calculated in the plane of the electroincision from the third trial using the fulgurate function at 50W.

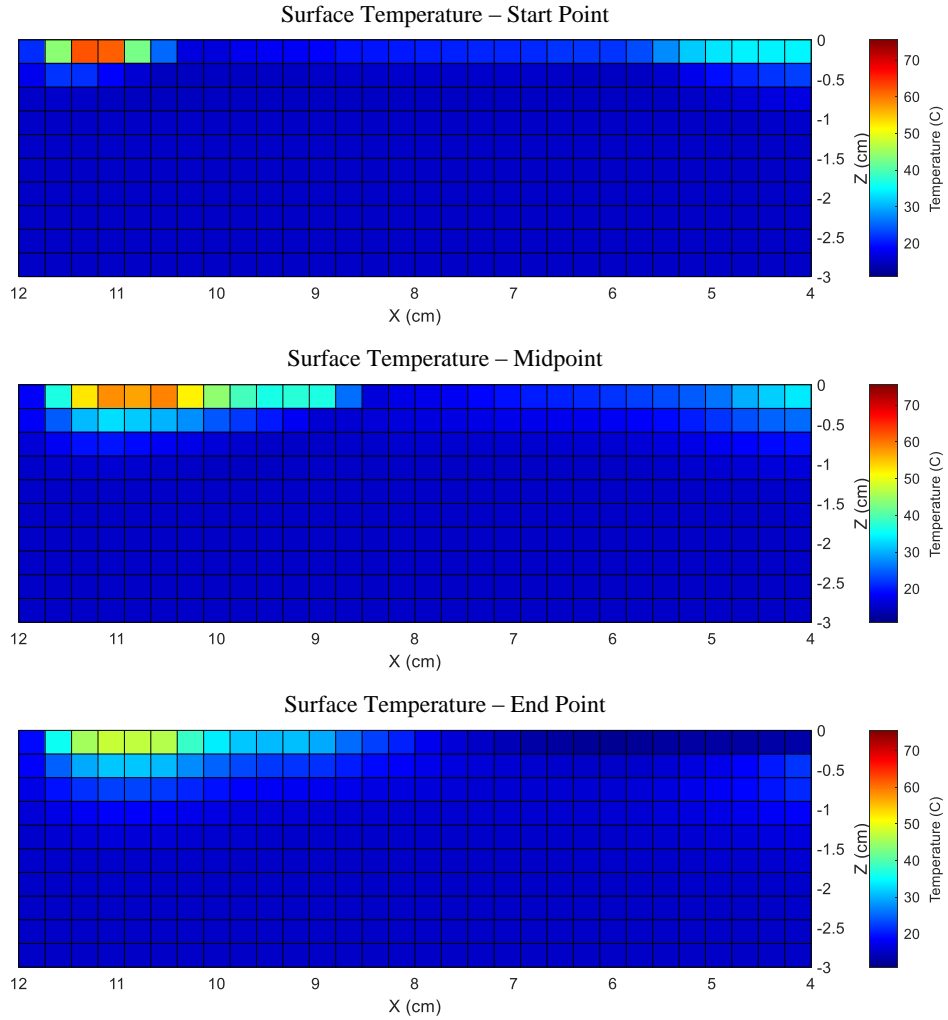


Figure 4.2.13 Temperature data calculated in the plane of the electroincision from the fourth trial using the fulgurate function at 50W.

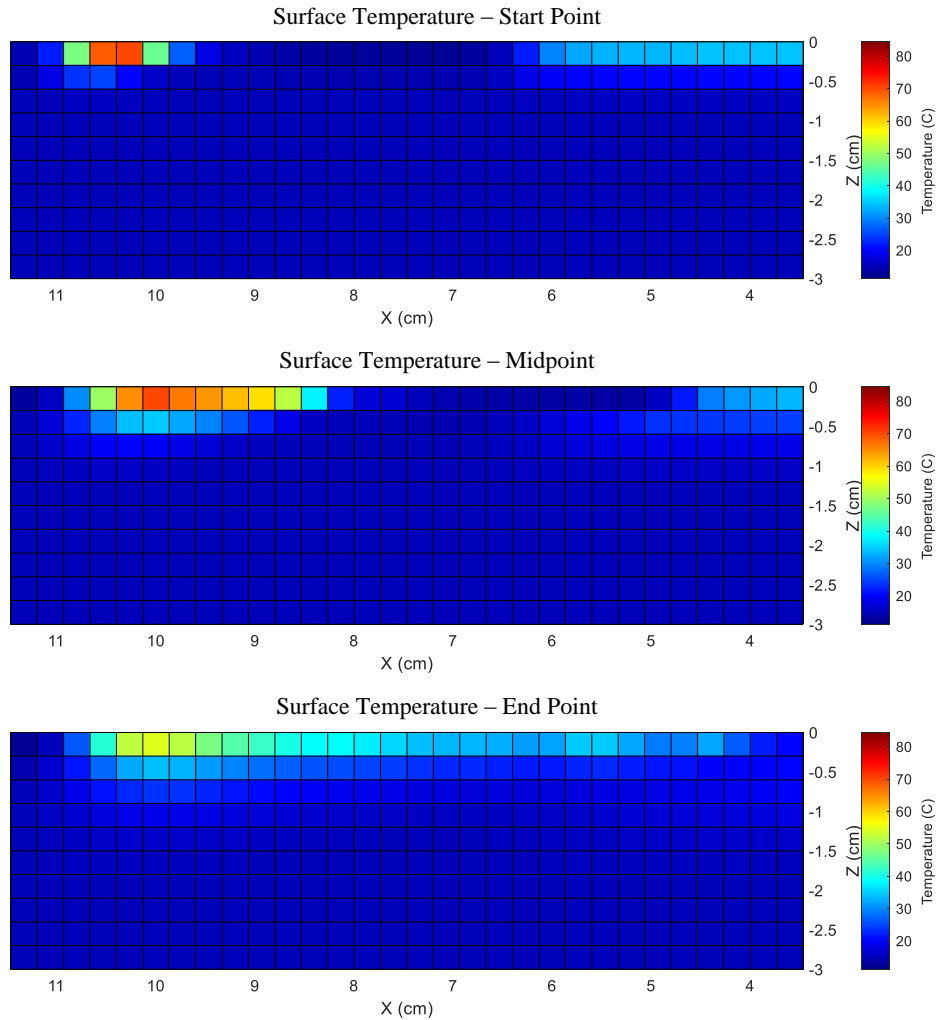


Figure 4.2.14 Temperature data calculated in the plane of the electroincision from the fifth trial using the fulgurate function at 50W.

Figure 4.2.15 and Figure 4.2.16 show the temperatures gradient in the x-z plane along the electroincision at the start point of the electroincision, during a midpoint of the electroincision, and during the conclusion of the electroincision for the trials made using the cut function set to 30W. Here, red coloring indicates temperatures around 35°C and blue coloring indicates temperatures around 10°C.

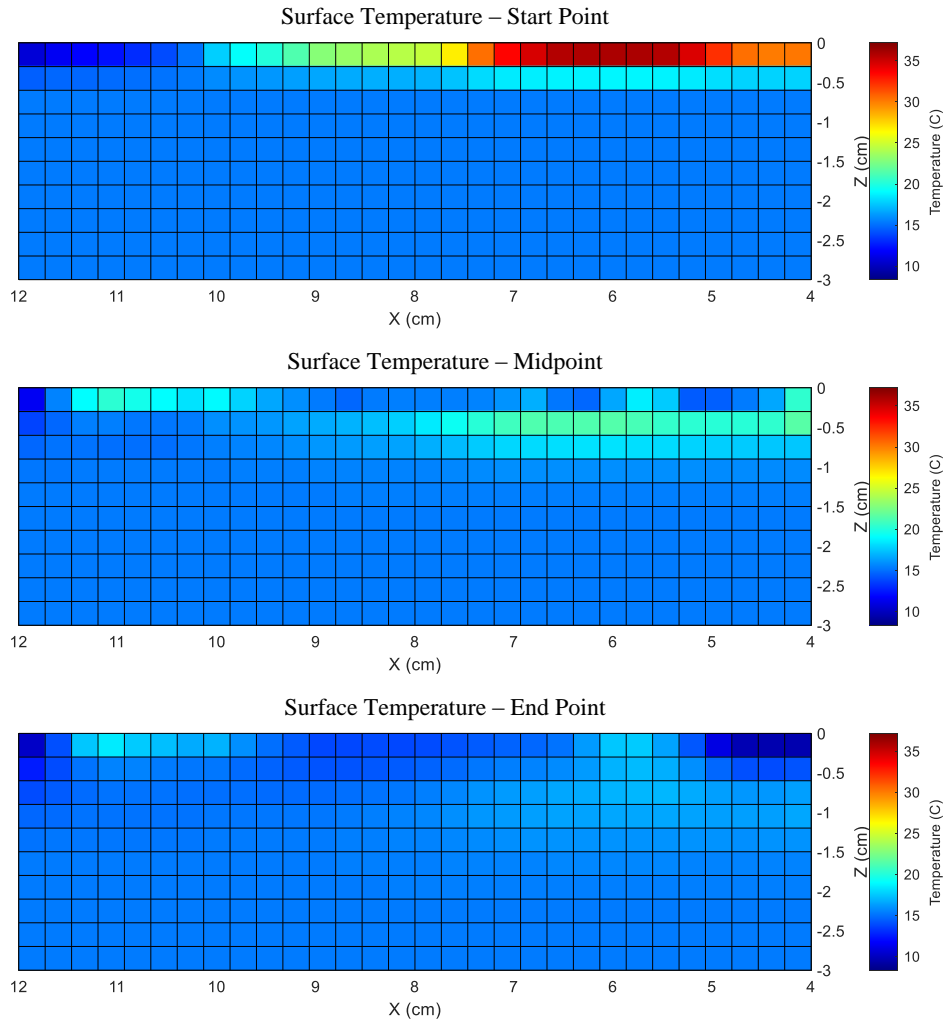


Figure 4.2.15 Temperature data calculated in the plane of the electroincision from the first trial using the pure cut function at 30W.

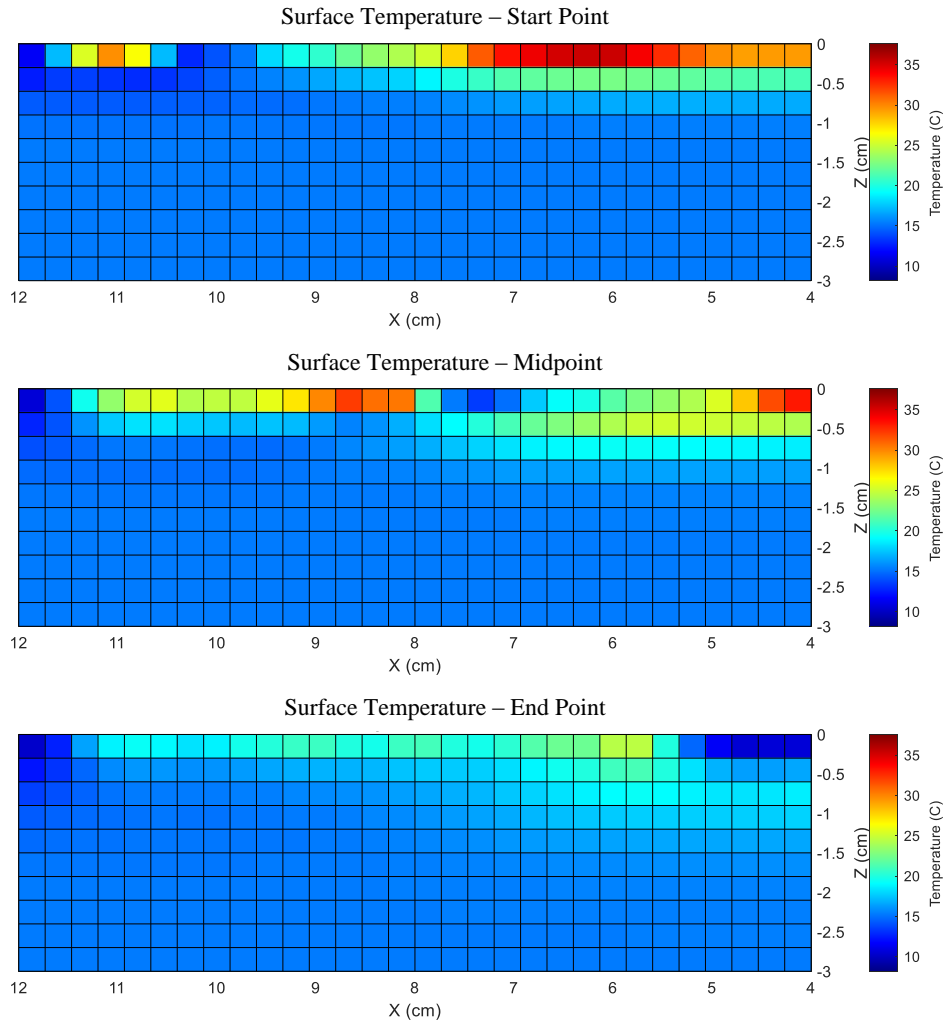


Figure 4.2.16 Temperature data calculated in the plane of the electroincision from the second trial using the pure cut function at 30W.

4.3 Tissue Damage Algorithm Results

Volumetric elements in Figure 4.3.1 through Figure 4.24 colored white show volume elements of healthy tissue, cells colored grey show volume elements that have sustained damage as a result of protein denaturation, and volume elements colored black represent areas of tissue that are non-viable and considered dead due to desiccation.

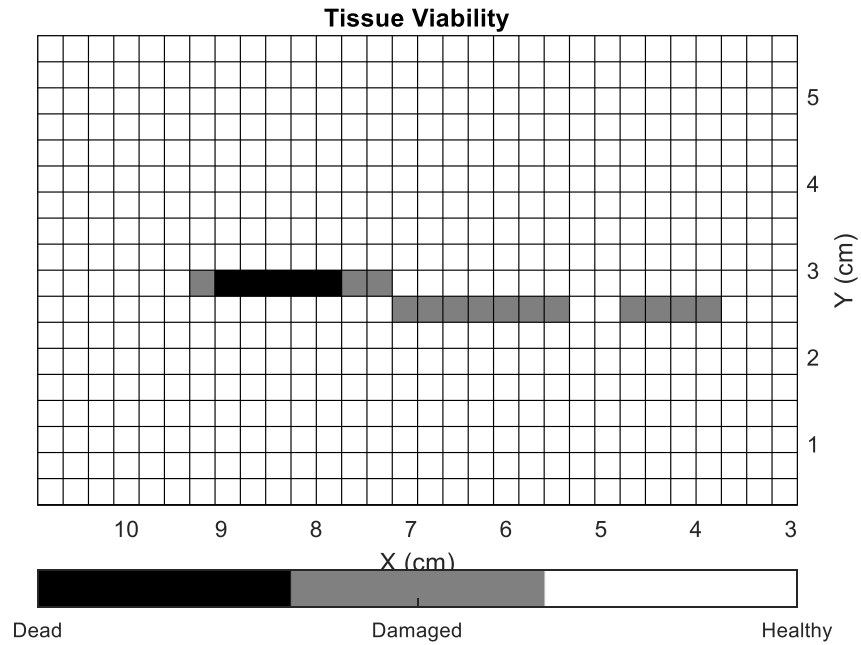


Figure 4.3.1 Tissue viability for the first trial using the fulgurate function at 50W.

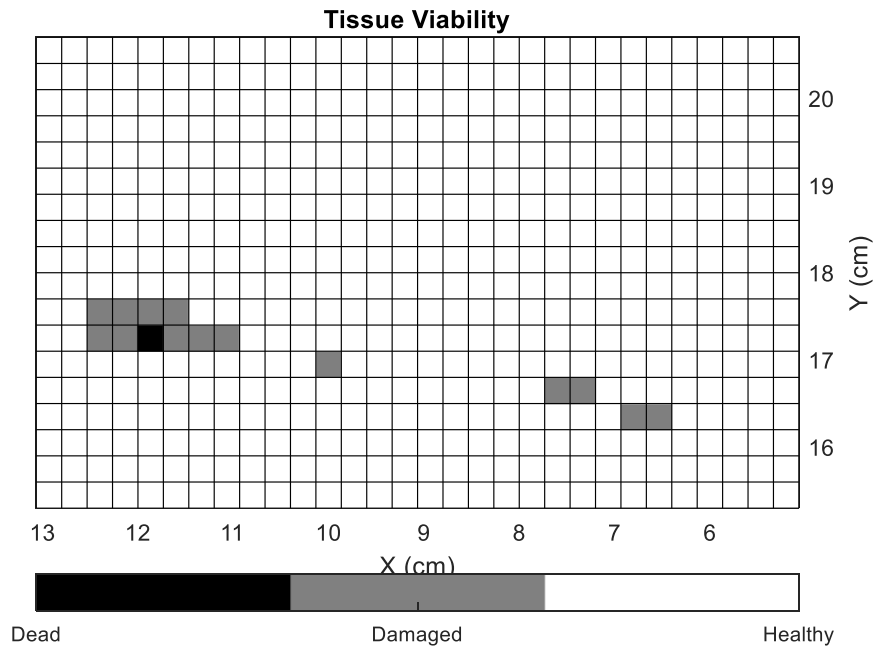


Figure 4.3.2 Tissue viability for the second trial using the fulgurate function at 50W.

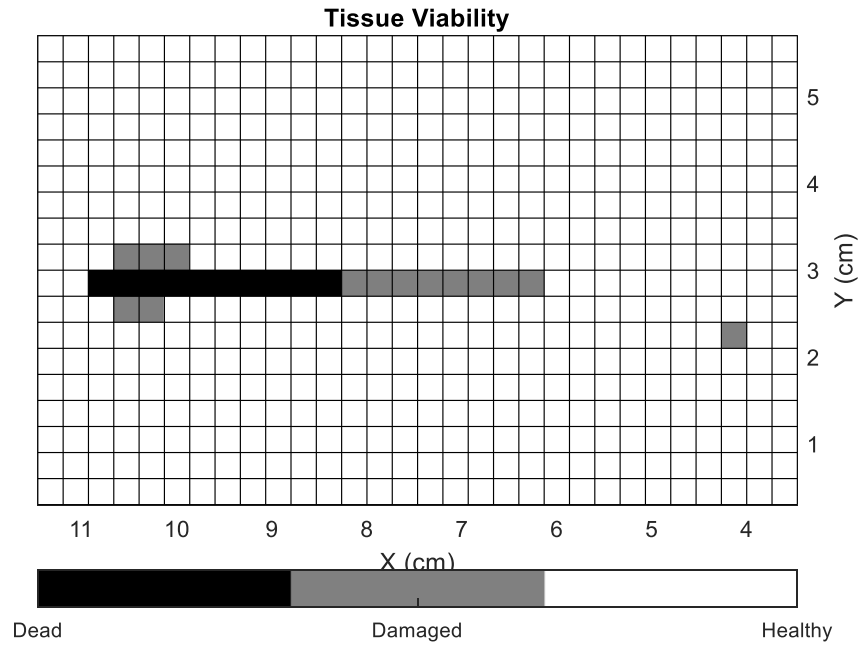


Figure 4.3.3 Tissue viability for the third trial using the fulgurate function at 50W.

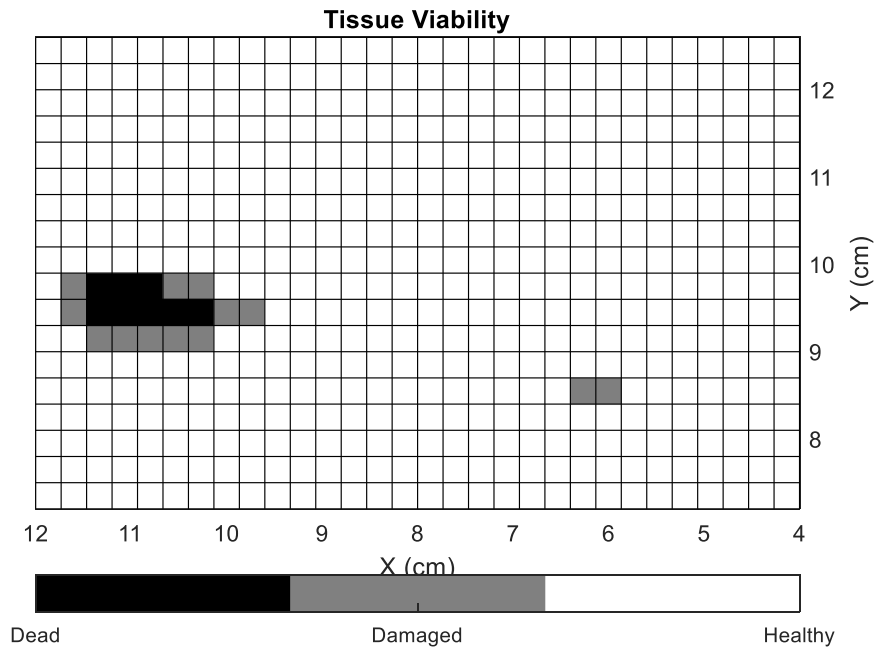


Figure 4.3.4 Tissue viability for the fourth trial using the fulgurate function at 50W.

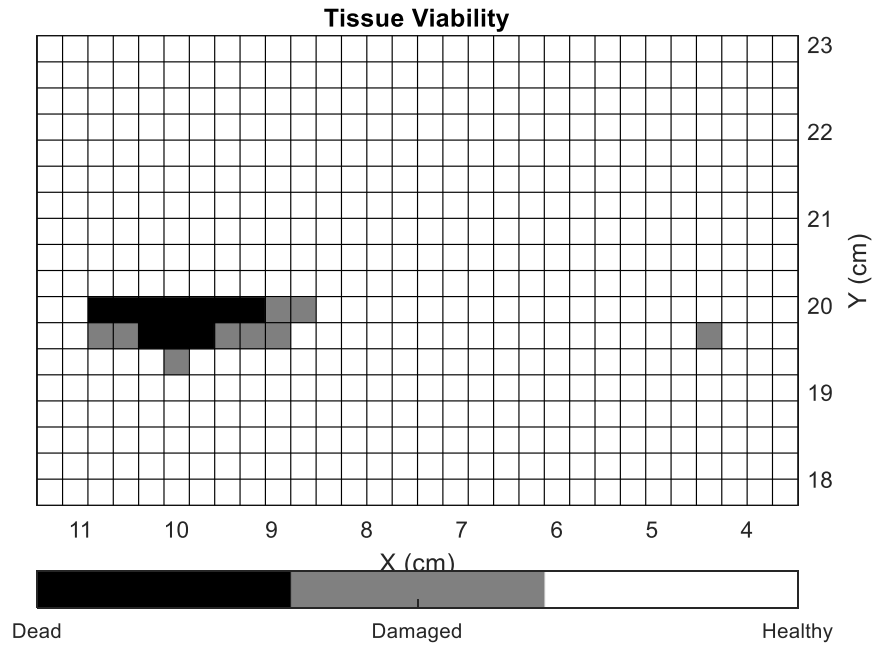


Figure 4.3.5 Tissue viability for the fifth trial using the fulgurate function at 50W.

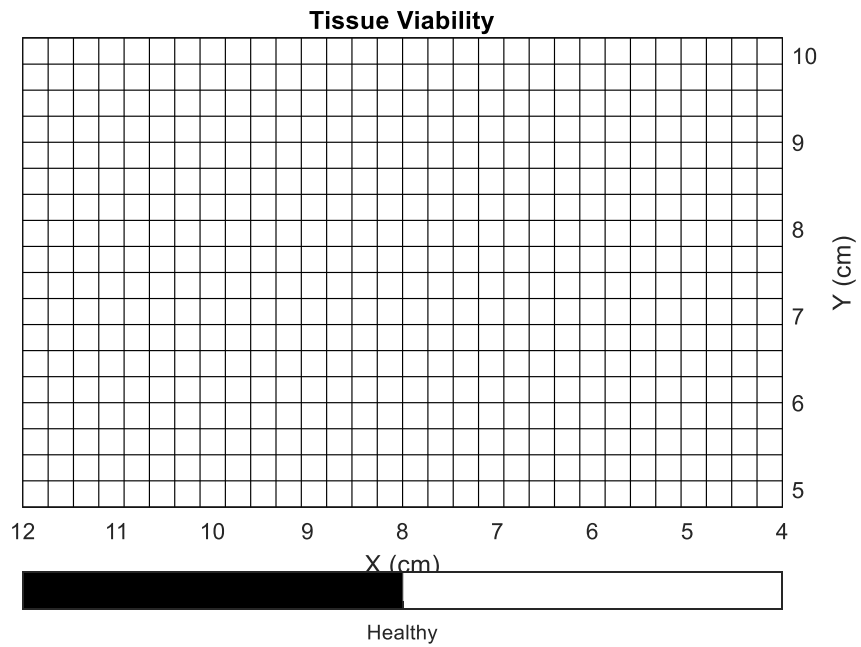


Figure 4.3.6 Tissue viability for the first trial using the pure cut function at 30W.

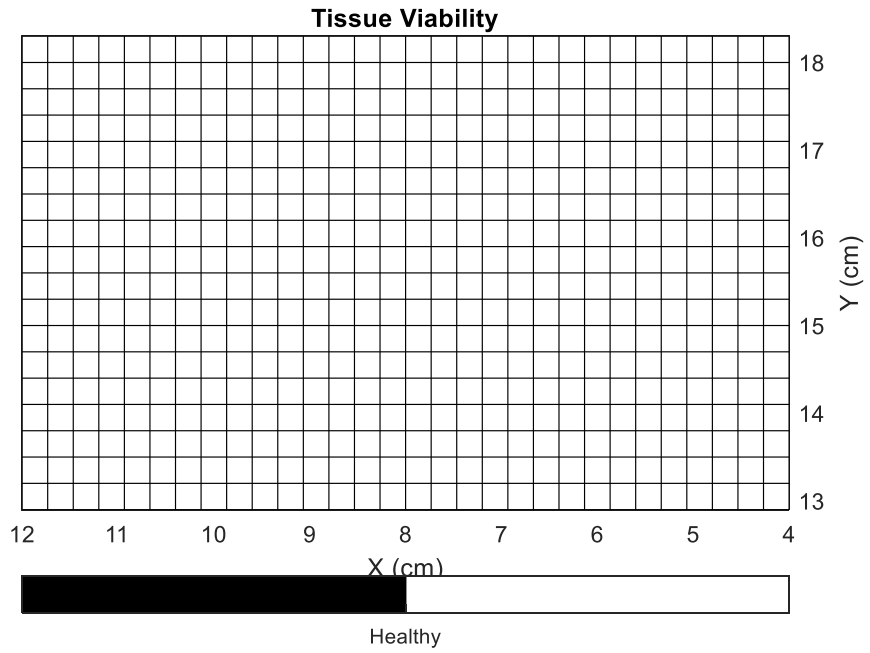


Figure 4.3.7 Tissue viability for the second trial using the pure cut function at 30W.

CHAPTER 5

DISCUSSION

The direct measurement of temperature at the pure cut function at 30W and the fulgurate function at 50W shows that there is a higher temperature increase using the fulgurate function, as shown in Figure 4.2.9. The maximum temperature of the volumetric element in the fulgurate setting trial is about 100°C, while the maximum temperature using the recommended cutting setting is only near 20°C. This means that the fulgurate setting increases the temperature in the volumetric elements by 80°C, a difference of four times between the settings. This could be expected, as when the fulguration function is set to 50W the peak voltage is 2800V, while in the pure cut mode at 30W, the peak voltage is 200V voltage. Similar trends are confirmed through all the comparisons between the trials using the fulgurate function at 50W and the pure cut function at 30W, they can be seen in Figure 4.2.2 through Figure 4.2.8.

Within the sensitivity of the thermograph camera the lateral temperature increases along the electroincisions of the pure cut setting trials are not observed. However, temperature increases are observed in the trials using the fulgurate function. In turn, the lower temperatures observed in the trials using the pure cut function, when processed by the tissue damage algorithm, correlate to no tissue damage or tissue death as seen in Figure 4.3.6 and Figure 4.3.7. In contrast, the high temperatures in the trials using the fulgurate setting lead to varying regions of both tissue damage and death as seen in Figure 4.3.1 through Figure 4.3.5. It should be also noted that in all cases using the fulgurate function, the tissue damage was computed to be highest at the initial insertion of the device as seen in Figure 4.2.5. On average, 1.5cm of the 6cm made on the porcine tissue model was predicted to be composed of dead tissue. In these cases, the area of necrosis and damage spans approximately 5mm perpendicular to the incision if it is assumed the incision is made through the center of the volumetric elements. From the thermal gradient calculations in the z direction, it

is seen that no additional tissue damage is caused below a depth of 3mm. This is most likely due to the starting temperature of the model being 15°C. An increase in thermal propagation along the z axis, and corresponding tissue damage or cell death predicted by the damage algorithm, would mostly likely be seen in a model starting at body temperature, 37°C.

CHAPTER 6

CONCLUSION

The high amount of thermal energy elicited into the biological system surrounding the electroincision can impact the viability of tissue. Based on previous studies a method for quantification of cell damage and cell death was developed. While all the specific mechanisms have not yet been identified, temperatures above 45°C result in partial tissue damage and temperatures above 60°C result in cell death. A thermal diffusion model in three dimensions was developed that allowed the prediction that the use of electrosurgical tools set to fulgurate at 50W and pure cut at 30W result in two distinct consequences to tissue. The results show that the electroincisions made with the recommended settings, 30W in pure cut, induce resulting temperatures of approximately 20°C in the surrounding tissue, staying well under the 45°C threshold of cell damage, predicting no damage to the tissue. The electroincisions made with 50W in fulgurate setting exhibit higher temperature spikes and commonly pass the 60°C cell death threshold. With the tissue damage model at 15°C there was very little damage below the model surface. These results emphasize the importance of electrosurgical tool settings in controlling the damage to surrounding tissue. Doing so may have an impact on the reduction of high infection rates, patient experience as well as alleviate the healthcare system of the associated costs.

CHAPTER 7

FURTHER CONSIDERATION

The following items have been considered for refinement and further consideration.

- Porcine model testing with a starting temperature of 37°C should be performed.
- In the case of caesarian delivery procedures, in order to ensure that the thermograph camera does not interfere with the physician's ability to perform the operation, it must be positioned further away from the site of electroincision. At greater distances, greater resolution is required to retain the same detail.
- The abdomen of a pregnant woman is a curved area, becoming more complicated as the site of injury is opened to allow the surgeon to cut deeper into tissue. To account for this complex geometry, the use of additional thermograph cameras and new mapping algorithms would need to be employed.
- In the case of hysterectomy, a laparoscopic thermograph device would need to be developed to study the deposit of thermal energy in the tissue surrounding the site electroincision.
- The addition of histological examination relating tissue changes to specific volume elements would be required to further develop the tissue damage algorithm. The denaturation of proteins and destruction of fat, along with charring caused during electroincision may also create an environment in the tissue that encourages bacterial growth. Structures such as lymph and blood vessels may be negatively impacted and have negative long-term effect on the tissue they are meant to supply.

APPENDIX
MATERIALS OUTLINE

Tables A.1 to A.3 describe the properties of the materials and equipment used.

Table A.1 Properties of the Thermograph Camera

Property	Description
Model Name	Flir C2
Frames per second	15 fps
Thermal Resolution	60x80 pixels
Temperature Range	-20°C to 180°C

Table A.2 Properties of the Thermocouple Datalogger Thermometer

Property	Description
Model Name	SE-520 Perfect Prime Data Logger Thermometer
Sample Rate	2 samples per second
Temperature Range (with Type K thermocouple)	-200°C to 1300°C

Table A.1 Properties of the Electrosurgery Equipment

Property	Description
Electrosurgical Generator Reference	COVIDIEN Force FX-CS
Rocker Switch Pencil Reference	COVIDIEN E2515H
Electrocautery Fine Tip Pen Reference	Cardinal Health Cat. 65410-181

APPENDIX B

MATLAB CODE

Below is a collection of the MATLAB codes used to calculate the thermal gradients of the tissue sample and to compute and relate the tissue damage information.

TEMPERATURE GRADIENT COMPUTATION

```
clear; clc; %data and command clear
```

```
load('Test_3_4.mat'); %data load
```

```
L = 0.16; W = .24; Th = .03; %m %length, width, thickness
```

```
Nz = 10; %number of z divisions
```

```
dz = Th/Nz; %m %size of z divisions
```

```
Ny = 60; %number of y divisions
```

```
dy = L/Ny; %m %size of y divisions
```

```
Nx = 80; %number of x divisions
```

```
dx = W/Nx; %m %size of x divisions
```

```
FC = length(data)/Ny; %frame count
```

```
dt = 1/15; %s %time interval
```

```
TA = 27; %C %atmospheric temperature
```

```
ST = 15.43; %C %starting model temperature
```

```

k = .23; %(W/m*K) %thermal conductivity

T = ST*ones([(Ny+2),(Nx+2),(Nz+1),FC]); %starting T matrix, [y,x,z,t]

%assigning boundary conditions

%atmospheric conditions

T(1, :, :, :) = TA;

T(Ny+2, :, :, :) = TA;

T(:, 1, :, :) = TA;

T(:, Nx+2, :, :) = TA;

%data conditions

for x = 1:FC

    T(2:Ny+1, 2:Nx+1, 1, x) = data(((60*(x-1)+1):(60*x)), (1:80));

end

%temperature gradient calculation

K = ones([(Ny+1),(Nx+1),(Nz),FC]);

K(:, 1, :, :) = (dy*dz)/(dx/2*k);

K(:, Nx+2, :, :) = (dy*dz)/(dx/2*k);

K(1, :, :, :) = (dx*dz)/(dy/2*k);

K(Ny+2, :, :, :) = (dx*dz)/(dy/2*k);

K(:, :, Nz+1, :) = (dx*dy)/(dz/2*k);

K(:, (2:Nx+1), :, :) = (dy*dz)/(2*(dx/2*k));

K((2:Ny+1), :, :, :) = (dx*dz)/(2*(dy/2*k));

```

```
K(:,:,1:Nz,:) = (dx*dy)/(2*(dz/2*k));
```

```
for f = 1:FC
```

```
    for k = 2:Nz
```

```
        for i = 2:Nx+1
```

```
            for j = 2:Ny+1
```

```
                H(j,i,k,f) = (K(j+1,i,k,f)*(T(j+1,i,k,f)-T(j,i,k,f)))+(K(j-1,i,k,f)*(T(j-1,i,k,f)-  
T(j,i,k,f)))+(K(j,i+1,k,f)*(T(j,i+1,k,f)-T(j,i,k,f)))+(K(j,i-1,k,f)*(T(j,i-1,k,f)-  
T(j,i,k,f)))+(K(j,i,k+1,f)*(T(j,i,k+1,f)-T(j,i,k,f)))+(K(j,i,k-1,f)*(T(j,i,k-1,f)-T(j,i,k,f)));
```

```
                C(j,i,k,f) = (dt*(K(j+1,i,k,f)+K(j-1,i,k,f)+K(j,i+1,k,f)+K(j,i-  
1,k,f)+K(j,i,k+1,f)+K(j,i,k-1,f)))/(dx*dy*dz);
```

```
                T(j,i,k,f+1) = T(j,i,k,f)+((dt/(C(j,i,k,f)*(dx*dy*dz)))*H(j,i,k,f));
```

```
            end
```

```
        end
```

```
    end
```

```
end
```

```
XU = (0:(W/Nx):(W-(W/Nx))); YV = (0:(L/Ny):L-(L/Ny)); ZW = (0:-:(Th/Nz):-Th); %x,  
y and z divisions
```

```
filename = 'Acc_3_4.mat';
```

```
save(filename)
```

TISSUE DAMAGE ALGORITHM

```
close all; clear; clc;
```

```
load('Acc_2_1.mat');
```

```
Crit = 60; Fail = 45;
```

```
for f = 1:FC
```

```
    for k = 1:Nz
```

```
        for i = 2:Nx+1
```

```
            for j = 2:Ny+1
```

```
                if f > 1 && T(j,i,k,f) < Crit && DD(j,i,k,f-1) == -1
```

```
                    DD(j,i,k,f) = -1;
```

```
                elseif f > 1 && T(j,i,k,f) < Crit && DD(j,i,k,f-1) == 0
```

```
                    DD(j,i,k,f) = 0;
```

```
                elseif T(j,i,k,f) >= Crit
```

```
                    DD(j,i,k,f) = -1;
```

```
                elseif T(j,i,k,f) < Crit && T(j,i,k,f) >= Fail
```

```
                    DD(j,i,k,f) = 0;
```

```
                elseif T(j,i,k,f) < Fail
```

```
DD(j,i,k,f) = 1;
```

```
end
```

REFERENCES

- [1] J. A. Martin, B. E. Hamilton, M. J. K. Osterman, A. K. Driscoll, and P. Drake, "Births: Final Data for 2017," cdc.gov, [Online]. Available: https://www.cdc.gov/nchs/data/nvsr/nvsr67/nvsr67_08-508.pdf
- [2] Centers for Disease Control Surgical Site Infection (SSI) Event. 2018. <https://www.cdc.gov/nhsn/pdfs/pscmanual/9pscasicurrent.pdf>. Accessed March 13, 2018
- [3] Conner SN, Verticchio JC, Tuuli MG, et al. Maternal obesity and risk of postcesarean wound complications. *Am J Perinatol* 2014;31:299–304
- [4] M.A. Olsen, A.M. Butler, D.M. Willers, G.A. Gross, and V.J. Fraser. (2013). Comparison of Costs of Surgical Site Infection and Endometritis after Cesarean Section Using Claims and Medical Record Data. *Infection Control and Hospital Epidemiology*. [Online]. Available: <https://www.ncbi.nlm.nih.gov/pmc/articles/PMC3618676/>
- [5] Whiteman MK, Hillis SD, Jamieson DJ, et al. Inpatient hysterectomy surveillance in the United States, 2000-2004. *Am J Obstet Gynecol*. 2008;198: 34 e1–34 e7.
- [6] Nieboer TE, Johnson N, Lethaby A, Surgical approach to hysterectomy for benign gynaecological disease. *Cochrane Database Syst Rev*. 2009; 3: CD003677.
- [7] Webster, J. G., & Clark, J. W. (1998). *Medical Instrumentation: Application and Design*. New York: Wiley.
- [8] Dr R.S. Khandpur. HANDBOOK OF BIOMEDICAL INSTRUMENTATION, THIRD EDITION. Instruments for Surgery, Chapter (McGraw Hill Education (India) Private Limited: New York, Chicago, San Francisco, Athens, London, Madrid, Mexico City, Milan, New Delhi, Singapore, Sydney, Toronto, 2014). <https://www.accessengineeringlibrary.com/content/book/9789339205430/chapter/chapter27>
- [9] Lee, J. (n.d.). Update on Electrosurgery. Retrieved April 4, 2020, from <https://www.outpatientsurgery.net/issues/2002/02/update-on-electrosurgery>
- [10] Davison, J, Zama, N, *Glob. libr. women's med.*, (ISSN: 1756-2228) 2008; DOI 10.3843/GLOWM.10021
- [11] Jones, D. B., Brunt, L. M., Feldman, L. S., Mikami, D. J., Robinson, T. N., & Jones, S. B. (2015). Safe energy use in the operating room. *Current Problems in Surgery*, 52(11), 447–468. doi: 10.1067/j.cpsurg.2015.08.004
- [12] Oconnor, J. L., & Bloom, D. A. (1996). William T. Bovie and electrosurgery. *Surgery*, 119(4), 390–396. doi: 10.1016/s0039-6060(96)80137-1
- [13] Mursano, L. S. (2013). Principles of Electrocautery [PowerPoint slides]. Retrieved from <https://louisville.edu/medicine/departments/medicine/divisions/gimedicine/physician-resources/lectures/procedures/electrocautery>

- [14] Taheri, A., Mansoori, P., Sandoval, L. F., Feldman, S. R., Pearce, D., & Williford, P. M. (2014). Electrosurgery. *Journal of the American Academy of Dermatology*, 70(4). doi: 10.1016/j.jaad.2013.09.056
- [15] Bovie Medical Corporation. (2013). *Aaron 3250 Electrosurgical Generator User's Guide*.
- [16] Cruse PJE, Foord R: A five year prospective study of 23,649 surgical wounds. *Arch Surg* 107: 206, 1973
- [17] Pearlman NW, Steigman GV, Vance V et al: A prospective study of incisional time, blood loss, pain and healing with carbon dioxide laser, scalpel, and electrosurgery. *Arch Surg* 126: 1018, 1991
- [18] Miller E, Paull DE, Morrissey K et al: Scalpel versus electrocautery in modified radical mastectomy. *Am Surg* 54 (5): 284, 1988
- [19] Siddaiah-Subramanya, M., Tiang, K. W., & Nyandowe, M. (2017). Complications, Implications, and Prevention of Electrosurgical Injuries: Corner Stone of Diathermy Use for Junior Surgical Trainees. *The Surgery Journal*, 03(04). doi: 10.1055/s-0037-1606547
- [20] Karacolak, T., Cooper, R., Unlu, E. S., & Topsakal, E. (2012). Dielectric Properties of Porcine Skin Tissue and In Vivo Testing of Implantable Antennas Using Pigs as Model Animals. *IEEE Antennas and Wireless Propagation Letters*, 11, 1686–1689. doi: 10.1109/lawp.2013.2241722
- [21] Summerfield, A., Meurens, F., & Ricklin, M. E. (2015). The immunology of the porcine skin and its value as a model for human skin. *Molecular Immunology*, 66(1), 14–21. doi: 10.1016/j.molimm.2014.10.023
- [22] T., B. (1996). *Heat conduction in two and three dimensions: Computer modelling of building physics applications*. Lund, Sweden.
- [23] El-Brawany, M. A., Nassiri, D. K., Terhaar, G., Shaw, A., Rivens, I., & Lozhken, K. (2009). Measurement of thermal and ultrasonic properties of some biological tissues. *Journal of Medical Engineering & Technology*, 33(3), 249–256. doi: 10.1080/03091900802451265
- [24] Dewhirst, M., Viglianti, B. L., Lora-Michiels, M., Hoopes, P. J., & Hanson, M. A. (2003). Thermal dose requirement for tissue effect: experimental and clinical findings. *Thermal Treatment of Tissue: Energy Delivery and Assessment II*. doi: 10.1117/12.476637
- [25] Hefermehl, L. J., Largo, R. A., Hermanns, T., Poyet, C., Sulser, T., & Eberli, D. (2014). Lateral temperature spread of monopolar, bipolar and ultrasonic instruments for robot-assisted laparoscopic surgery. *BJU International*, 114(2), 245–252. doi: 10.1111/bju.12498
- [26] Sakiyama, T., Han, S., Torii, A., Miyawaki, O., & Yano, T. (1991). Intrinsic thermal conductivity of gelatin estimated independently of heat conduction models. *Agricultural and Biological Chemistry*, 55(2), 487–492. doi: 10.1271/bbb1961.55.487